TOWARDS FIELD SCALE IN-SITU COMBUSTION SIMULATION

A THESIS SUBMITTED TO THE DEPARTMENT OF
ENERGY RESOURCES ENGINEERING
OF STANFORD UNIVERSITY
IN PARTIAL FULFILLMENT OF THE REQUIREMENTS FOR
THE DEGREE OF MASTER OF SCIENCE

Guenther Glatz

May 2012

© Copyright by Guenther Glatz 2012
All Rights Reserved

I certify that I have read this thesis and that in my opinion it is fully adequate, in scope and in quality, as partial fulfillment of the degree of Master of Science in Energy Resources Engineering.

(Anthony R. Kovscek) Principal Adviser

I certify that I have read this thesis and that in my opinion it is fully adequate, in scope and in quality, as partial fulfillment of the degree of Master of Science in Energy Resources Engineering.

(Louis Castanier)

Abstract

This master thesis increases understanding of ISC mechanisms based on experimental results for a Central European crude for which ISC has proven to be economically successful. Ramped temperature oxidation (RTO), or so-called kinetics, studies measure the rate of crude-oil oxidation. Similarly, combustion tubes packed with mixtures of sand, clay, water, and hydrocarbon measure our ability to propagate a combustion front. Through the combination of the isoconversional approach for an initial estimation of reaction kinetics (apparent activation energy E_a, Arrhenius constant pre-exponential factor A) and implementation of combustion tube runs under different conditions, the mechanisms behind the combustion process are elucidated. The results of seven combustion tube runs are presented and discussed in terms of repeatability, effect of grain surface area, gas concentration oscillations, stoichiometry, minimum air flow-rate and recovery efficiency. Based on experimental results, crucial parameters for field application as well as for simulation are derived (hydrogen/carbon-ratio, air requirements).

Opposed to previous publications, the ISC process is described in terms of stoichiometry for the entire tube run, giving insight in development of hydrogen/carbon-ratio and other important parameters over time. This helps to compare, verify, and tune simulation results obtained from commercial simulators.

Results obtained point out the exceptional efficiency in terms of recovery. Monitoring combustion stoichiometry over time gives an increased insight in flue-gas composition oscillations.

In addition, measures to render in-situ combustion field scale simulation possible using commercial software are discussed.

Acknowledgements

I would like to express my sincere gratitude to my advisers Prof. Anthony Kovscek and Dr. Louis Castanier for their time, confidence, support and guidance. None of this would have been possible without them. Their comments and suggestions were extremely valuable to my research. I would also like to thank Murat Cinar and Berna Hasçakir for their useful input and help regarding experiments. I am grateful to OMV and Torsten Clemens for the financial support for this research. I am grateful to my family and my wife who supported me during my study.

Contents

List of Tables

List of Figures

Chapter 1

Introduction

Despite an increased commitment to renewable energy, the world continues to rely heavily on fossil hydrocarbons as a main energy resource. According to the International Energy Outlook [32], world marketed energy consumption grows by 49% from 2007 to 2035. Furthermore, world use of liquids and other petroleum grows from 86.1 million barrels per day in 2007 to 92.1 million barrels per day in 2020, 103.9 million barrels per day in 2030, and 110.6 million barrels per day in 2035. In order to meet the projected increase in world demand in the Reference case, liquids production (including both conventional and unconventional liquid supplies) needs to increase by a total of 25.8 million barrels per day from 2007 to 2035. Sustained high oil prices allow unconventional resources (including oil sands, extra-heavy oil, biofuels, coal-to-liquids, gas-to-liquids, and shale oil) to become economically competitive. Consequently world production of unconventional liquid fuels, that totalled only 3.4 million barrels per day in 2007, is assumed to increase to 12.9 million barrels per day accounting for 12% of total world liquids supply in 2035. According to http://www.heavyoilinfo.com/, unconventional resources account for about 70% of total world oil resources. Canada and Venezuela alone are estimated to have unconventional resources exceeding the conventional resources by far.

Depending on the type of unconventional resource different enhanced oil recovery (EOR) methods can be applied. In the case of thermal recovery processes, production is achieved by viscosity reduction through heat. The reservoir temperature is

increased locally by either injection of hot water, hot steam, or in-situ. Especially in the case of heavy-oil resources, in-situ combustion (ISC) or fire-flooding provides effective means to produce this resource in an economic and environmentally sound manner. Being not limited to heavy-oil reservoirs [46] the energy required to reduce the viscosity and displace the oil is generated in the reservoir by chemical reactions. Injected oxygen reacts with heavy fractions of the crude oil dramatically increasing the temperature and, therefore, reducing viscosity. In addition to viscosity reduction, gas drive and thermal expansion foster production [40]. Compared to other thermal recovery methods, ISC offers several advantages. First, the portion of the crude oil burned is likely to be the heaviest and least valuable [40]. Even more, the ISC process acts as a sort of refinery providing an upgrade in API gravity, reduction of heavy metals and reduction of sulfur content.

Though being one of the oldest thermal recovery methods, industry has been reluctant to apply ISC in the field for several reasons. Despite many economically successful field projects [10], the high number of failures of many early field trials led to the conception that ISC is a high risk operation. Especially the lack of reliable tools for efficient and accurate prediction of field performance indicates that, even after a century of application, the mechanisms behind ISC are not understood to their full extent. While technological advances made implementation of an ISC process on field scale more viable, modelling is still a significant problem. Currently simulation studies related to ISC are restricted to modeling small laboratory scale problems such as kinetics cell and combustion tube experiments. The transition from laboratory to field scale is still an unsolved problem due to the very nature of the ISC process in combination with the discretization techniques used to solve the reactive transport equations. For ISC, the chemical reaction front is physically very narrow and requires sub-inch-sized grids to be captured accurately. This is orders of magnitude smaller than affordable grid block sizes for full field reservoir models. Accordingly, severe grid size effects are encountered in full field scale simulation making performance predictions infeasible. Bazargan et al. [3] proposed a workflow to render field-scale simulation possible using commercial software. In this thesis a simplified version of the workflow is employed (see Fig. 1.1) in an effort to history match 40 years of

production of one of the worlds largest and most successful ISC projects located in Central Europe.

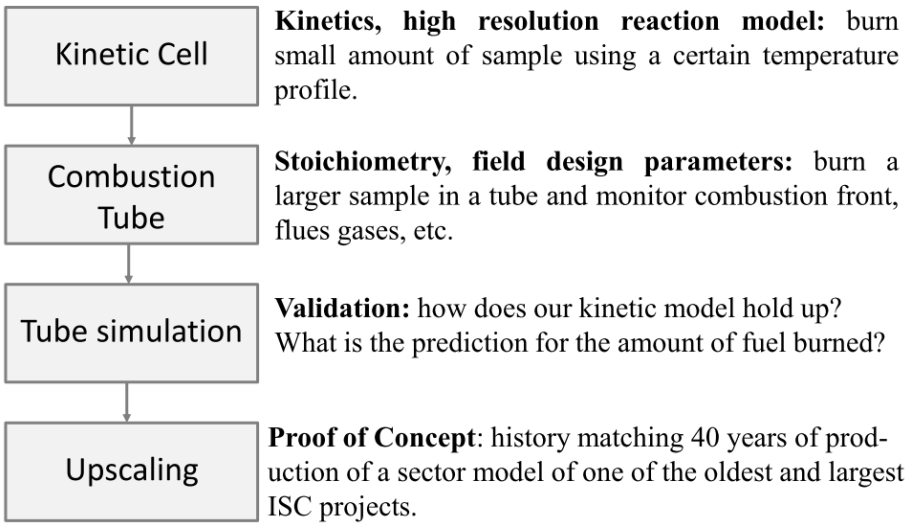

Figure 1.1: Simplified workflow from [3] for ISC simulation on field scale.

To establish parameter values for the kinetic models used in the numerical simulation of ISC processes, kinetic cell and combustion tube experiments provide a sound basis. Kinetic cell experiments help to determine the reaction kinetics that are defined as the study of rate and extent of chemical transformation of reactants to products (see Chapter 2). Combustion tube runs help to determine important parameters like equivalent hydrogen-carbon ratio (H/C ratio) and can give an idea of the stoichiometry for the high temperature oxidation process (see Chapter 3). The parameters obtained are then used in combustion tube and field-scale simulation respectively. Combustion tube simulations are not included in this thesis. Chapter 4 summarizes the steps taken for history matching oil production of a 300,000 cell sector model including 10 years of cold and 30 years of hot production.

Chapter 2

Kinetic Cell Experiments

Before completing combustion tube runs, it is vital to understand and determine the reaction kinetics of oxidation of reactants to products. The study of kinetics of crude-oil oxidation in porous media helps to characterize the reactivity of the oil, to determine the conditions required to achieve ignition, gain insight into the nature of fuel formed, and to establish parameter values for the kinetic models used in the numerical simulation [48].

In order to determine the kinetic parameters of the crude oil (pre-exponential factor, activation energy), several conventional methods like accelerated rate calorimetry [48] or thermogravimetric analysis [2] can be used. According to [9] the previously mentioned methods assume a reaction model to interpret experimental data that may lead to oversimplification. Kinetic parameters in this case, however, were determined based on the isoconversional method as described in [56] and applied to crude oil as shown by [12, 13, 14]. As pointed out in [21] combustion of crude oil in porous media is not a simple reaction but follows several consecutive and competing reactions occurring through different temperature ranges. In order to model the reactions that occur in a combustion process, an extended compositional analysis and a large number of kinetic expressions are required. An accurate description of the oxidation of the simplest hydrocarbon, methane, requires hundreds of reactions to be taken into account [48]. A similar level of detail for crude oil appears exceptionally difficult to develop. The activation energy calculated is *apparent*, *effective*, or *variable* in the

sense that it is a result of reactions occurring in parallel that are lumped together into one activation energy value [24, 54]. The isoconversional approach provides a model-free technique to estimate effective activation energy, is useful for screening of the likelihood of successful combustion, and suggests the global reactions governing ISC.

2.1 Experimental Apparatus and Procedures

Previous studies at Stanford have produced an experimental apparatus for both RTO and combustion tube experiments [22, 34, 41]. The system was upgraded by [12] (see Fig. 2.1).

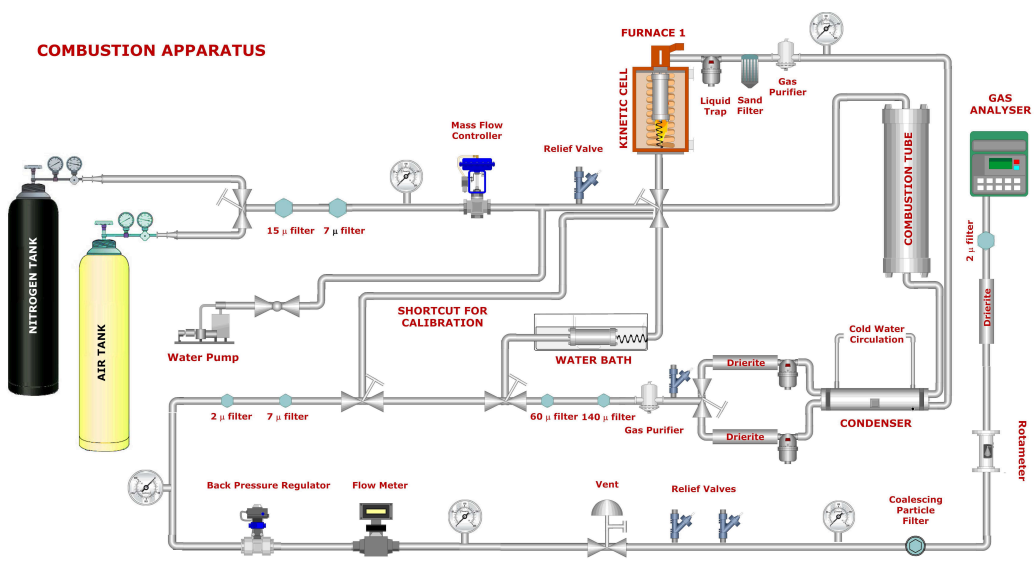

Figure 2.1: Experimental apparatus [12].

The sample was prepared to mimic reservoir conditions. Typically, 50.00 g of 60 mesh sand and 3.60g of powdered kaolinite were placed in a round bottomed dish and mixed using a spatula until evenly distributed (refer to Table A.5).[1] To achieve water-wet conditions, 4.00 g of distilled water were added and mixed until the the mixture was evenly moist. Care was taken to hold the dish at the top edge rather

[1] 60 mesh stands for 60 mesh and corresponds to a sieve size of 0.31 mm.

than at the bottom to prevent body heat fostering premature evaporation of water. Finally, 2.00 g of the crude oil under investigation were added and blended until a homogeneous mixture was obtained. The crude oil is 15.9 $API°$ and 2000 cP at 18°C.

Then, the sample was tamped into the kinetics cell using a plunger. A coarse 16 mesh sand provided inlet gas distribution.[2] With the sample in the kinetic cell, the end plugs were tightened. To guarantee leak-free operational conditions, the cell was flushed with nitrogen and the test pressure was gradually increased to approximately 150 psi. The pressurized cell was then submerged in a water bath to check for leaks. If no leaks were detected, the outside of the cell was dried and placed in the furnace. Thermocouples are used to measure temperature at three different points along the center of the cell and in the furnace to check for a uniform temperature distribution.

Before each experiment, all modules (CO_2, CO, CH_4, and O_2) of the gas analyzer were calibrated using high purity calibration gases. Care was taken to ensure that each module was subject to its calibration gas for a sufficient time. After the calibration was finished, the cell was pressurized to 100 psia corresponding to reservoir conditions. Additionally, connections were scrutinized for leaks using a detergent solution. The experiment was then started. Based on a pre-programmed heating schedule the temperature was increased linearly while air was passed through the cell at a flow rate of 2 l/min. The pressure at the inlet and the outlet of the cell, exit flow rate, temperature in the cell and furnace, and effluent gas composition were recorded continuously during the experiment.

As outlined in [13], the isoconversional technique requires a series of experiments to be conducted at different heating rates. All other parameters, such as pressure, flow rate, and initial temperature are held fixed for all tests. Each experiment is conducted with great care to achieve satisfactory and consistent results. Some variability does exist from run to run. For instance, water evaporates during sample preparation and some oil adheres to the surface of the dish.

[2] 16 mesh corresponds to a sieve size of 1.4 mm.

2.2 Post-Processing of Experimental Data and Diagnostic Plots

During the experiment effluent O_2, CO_2, and CO are recorded using a gas analyzer. Gas data cannot be used directly. The isoconversional principle requires conversion and, therefore, the oxygen consumption to be calculated. The problem is that the composition of the air used is not exactly 21% oxygen and 79% nitrogen. The oxygen concentration at the outlet is between 20.5% and 21% when no oxygen is consumed. Hence, a baseline must be determined not only for oxygen but for all gases measured. As a best practice, it was decided to determine the baseline by taking an average value from the gas readings up to one hour into the experiment. Any negative values were forced to zero. Unfortunately, the gas analyzer readings shift over time suggesting that oxygen is consumed even after all oil was burned (see Fig. 2.2 after three hours into the experiment). The variations in initial and final state of oxygen consumption are compensated by applying a technique originally used for background correction in X-ray Photoelectron Spectroscopy (XPS) data. In this case, the [52] algorithm is used to construct a background sensitive to changes in data.

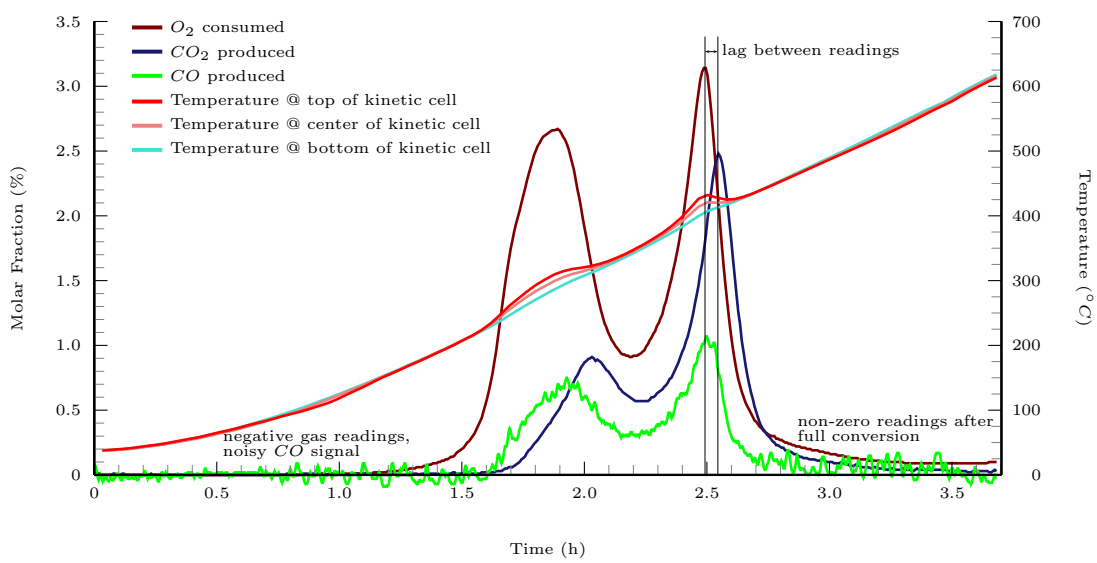

Figure 2.2: Example of RTO kinetics experimental results and measurement issues.

Fig. 2.2 also shows that the individual modules of the gas analyzer have lag

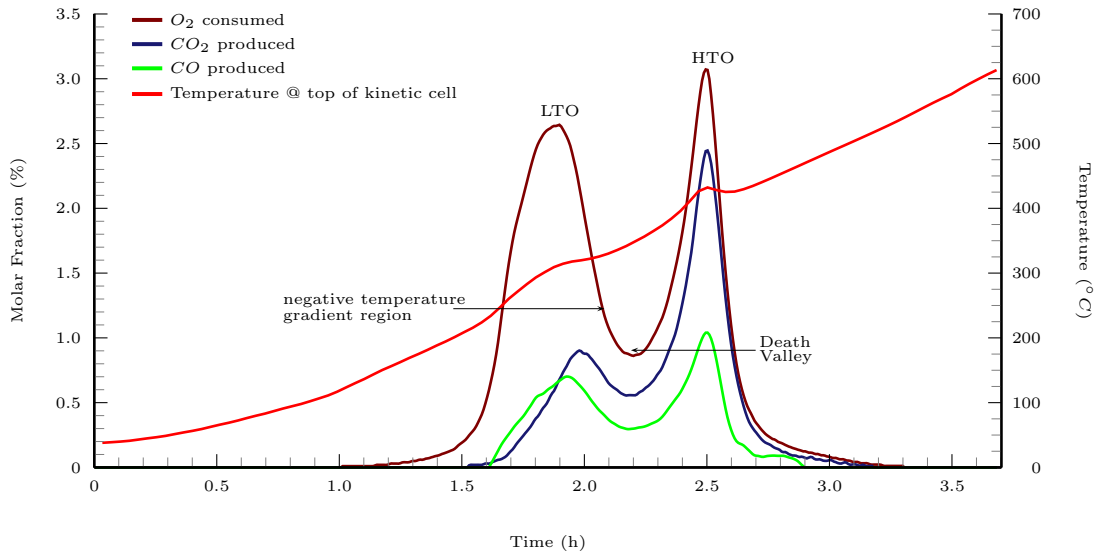

Figure 2.3: Example of corrected RTO kinetics experimental results.

relative to each other because of different types of sensors. The time difference is especially pronounced for oxygen and carbon dioxide. The carbon dioxide readings as well as the carbon monoxide readings had to be shifted with respect to oxygen readings. The carbon dioxide readings were filtered using a finite impulse response smoothing filter as described in [49]. In Fig. 2.3, the measured data was corrected using the methods described above. In comparison with Fig. 2.2, Fig. 2.3 shows no gas production/consumption after the experiment has finished and no lag between individual gas readings.

The burning behavior of the oil observed in Fig. 2.3 is comparable to other experimental results reported [6, 13, 35]. In the literature, two main regions are distinguished. Generally, low temperature oxidation (LTO) reactions occur below $\approx 350°C$ and are thought of as oxygen addition reactions yielding partially oxygenated compounds [6]. However, as pointed out in [37], the temperature range is oil dependent. The high temperature oxidation (HTO) reaction is the actual burning or bond-scission reaction i.e. the reaction between fuel and air injected. This reaction is believed to happen above $350°C$ [44]. LTO and HTO regions are separated by the negative temperature gradient region, also referred to as *Death Valley*.[3] In some cases, however,

[3]The term was coined by Prof. Gordon Moore at the University of Calgary.

LTO and HTO reactions were reported to overlap [1].

A distinctive part of the LTO region is the negative temperature gradient [39]. Although temperature increases, less and less oxygen is consumed. The fuel is then burned in the HTO region [44]. The sharp peak in oxygen consumption indicates that an extensive amount of conversion happens for a very small temperature window (from $400°C$ to $430°C$). For both, LTO and HTO reactions, an increase in temperature is observed (see Fig. 2.3). As mentioned before, the temperature is recorded at three different positions in the kinetic cell i.e. at the bottom of the cell (BOC), center of the cell (COC), and at the top of the cell (TOC). For the isoconversional analysis, always, the temperature profile yielding the greatest deviation from the programmed heating profile is used. Usually this is true for the uppermost thermocouple at the top of the cell (see Fig. 2.2). It is assumed that the reaction releasing the most heat is the dominant reaction. Therefore, when calculating effective activation energies, the profile giving the greatest temperature deviation is used to capture this/these reaction(s). Also, during the experiment it is assumed that the oil is pushed towards the upper part of the cell because air is injected from below. A temperature increase results in a viscosity decrease making it easier for the oil to move.

2.3 Kinetic Cell Results

For kinetic cell runs three different solid mixtures were taken into consideration to study the effect of surface area. First, experiments were carried out using production sand. Production sand refers to sand produced along with the oil and collected in the surface lines. Based on reservoir-core material, the mineralogy was investigated using X-Ray Diffraction Analysis. The results of these measurements are summarized in Table A.2 and Table A.3. Notably, the overall clay content is about 20%. The production sand used for investigation was contaminated with oil and had to be cleaned first using toluene. After all oil was removed, the sand was put into a vacuum oven at $38°C$ to ensure that all toluene was evaporated. Then, the sand was saturated with distilled water to re-hydrate any clays present that might have been affected by the toluene. Again the sand was put into a vacuum oven at $38°C$ until dry. Next

a sieving analysis was carried out using $\approx 580g$ of cleansed production sand. Sieve meshes from 14# up to 200# were available. Based on the results a grading curve was constructed and the diameters D_{10}, D_{30}, and D_{60} were determined. Furthermore, the uniformity coefficient C_u and coefficient of curvature C_c were calculated (see Table A.4). A histogram of the grain size data is given in Fig. 2.4.

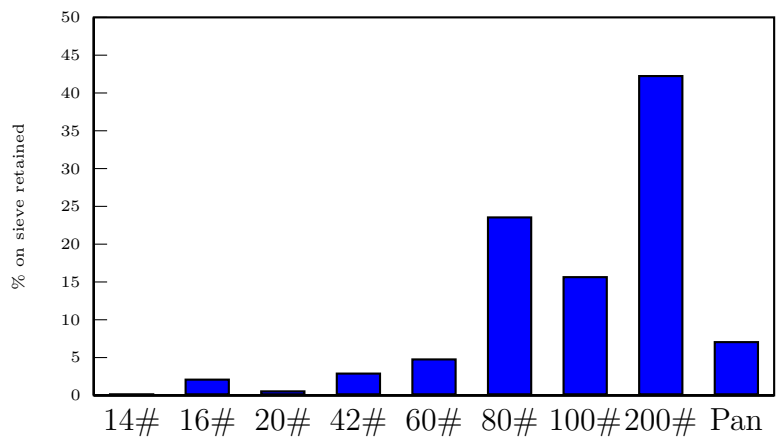

Figure 2.4: Histogram for sieve analysis.

Overall the sand shows a bimodal distribution with almost half of the grains having a size smaller than 0.075 mm. The solid mixture used for the kinetic cell runs shown in Fig. 2.5 is summarized in Table A.5.

The oxygen consumption for production sand summarized in Fig. 2.5 exhibits classic burning behavior (LTO, HTO etc.). In addition, we see complications, especially for the LTO region and smaller heating rates. During the LTO process, reactions create an additional boost in oxygen consumption. Also, at the end of the experiment a third hump is observed. The origin of the third hump is currently unknown.

Fig. 2.6 shows a plot of effective activation energies E_a versus conversion. Activation energy values were calculated using the Friedman method [23]. Though this method is based on calculating differentials and sometimes amplifies errors, Cinar et al. have determined that this method is applicable without problem. The 95% confidence interval is interpreted as follows: out of 100 experimental series, the

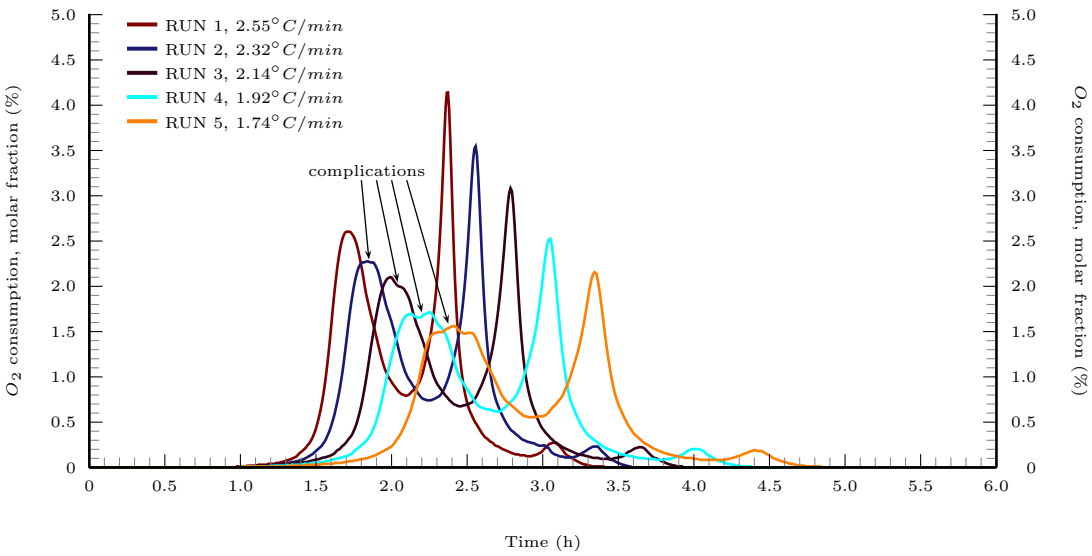

Figure 2.5: Oxygen consumption for crude oil/production sand mixture.

activation energy calculated for 95 of the experimental series yields activation energies within the range of the confidence interval. When calculating activation energies below 10% and above 90% care has to be taken because of numerical difficulties. Usually, these ranges give a very large spread for activation energy. In this case, however, a small confidence interval indicates that values calculated are very reliable.

In Fig. 2.6 the LTO region is within a conversion range of 0 to ≈ 0.3. The negative temperature gradient region ranges from ≈ 0.3 to ≈ 0.6 and the HTO region from ≈ 0.6 to ≈ 0.9. Ideally, activation energies for both the LTO and HTO regions are constant. In this case however, we can see several complications. Activation energies for the LTO reactions are only constant within a conversion range of 0.1 to 0.2, values from 0.0 to 0.1 and 0.2 to 0.35 vary. From past experience, reactions taking place within a conversion window of 0.0 to 0.1 do not contribute substantially to a reaction scheme and are, therefore, neglected. Reactions within the conversion window of 0.2 to 0.35, however, are of great importance and cannot be neglected. Modelling them properly is key to describe the process accurately. The sharp increase in activation energy at a conversion of 0.95 is associated with the third hump mentioned before.

Interpreting apparent activation energy on a conversion basis is hard to perceive conceptually. Plotting apparent activation energy versus average temperature is more

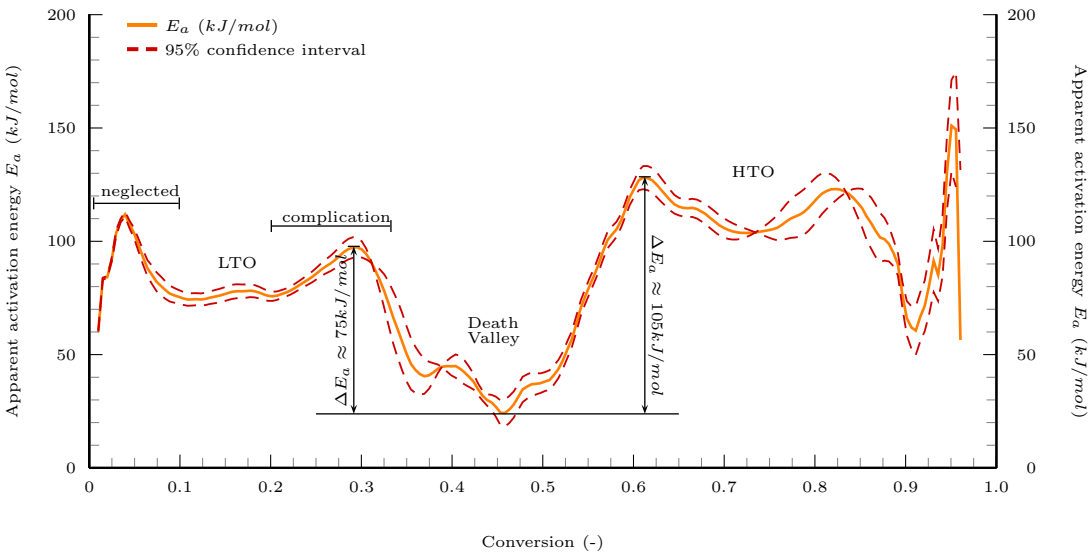

Figure 2.6: Apparent activation energy for crude oil/production sand mixture.

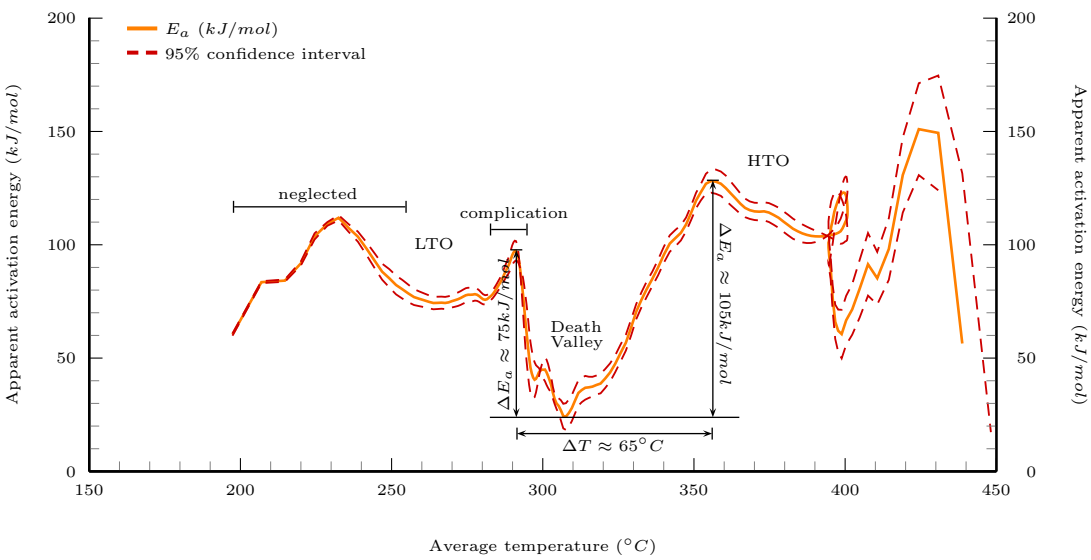

Figure 2.7: Apparent activation energy for crude oil/production sand mixture vs. average temperature.

helpful for identifying individual reactions that might be of interest when outlining a reaction scheme. In Fig. 2.7 apparent activation energy is plotted against temperature. First, we easily bracket the temperature window within which all reactions take place (here $200°C$ to $440°C$). Secondly, we single out important temperature ranges. The conversion range of 0.2 to 0.3 corresponds to a temperature window of only $10°C$ (from $285°C$ to $295°C$). Again, this stresses the importance to consider this event in the reaction scheme.

The LTO region occupies a temperature window of $\approx 100°C$ (from $200°C$ to $300°C$) whereas the HTO region is given for a comparably narrow window of $\approx 50°C$ (from $350°C$ to $400°C$). The HTO region also yields complications because activation energies decrease gradually rather than levelling out in a plateau.

From past experience it is known, that a successful tube run is a function of both crude oil and reservoir matrix properties. Cinar et al. reported a case of an oil unable to sustain a combustion front in the tube using the native reservoir rock. When combined with a different reservoir rock, however, the oil burned successfully. The isoconversional fingerprint shown in Fig. 2.6 and Fig. 2.7, respectively, are obtained for reservoir conditions. For this fingerprint, we know, that ISC is both technically and economically successful. Hence, the fingerprint provides a valuable reference case when comparing with oils that are screened for ISC using RTO experiments combined with isoconversional analysis. In order to increase our understanding of the impact of reservoir matrix on the burning behavior, additional kinetic cell runs using a reduced surface area were carried out.

In Fig. 2.8, the *original reservoir matrix* data series corresponds to the isoconversional fingerprint shown in Fig. 2.7. In addition, the results for two experimental kinetic cell series with increased surface area are plotted.A summary of solid/liquid mixtures used is given in Table A.5. For both *60 mesh sand/clay combination* and *16 mesh sand* the sand used was "cooked" i.e. burned in an oven to remove any contaminants that could possibly have an effect on burning behavior.

The *16 mesh sand* data series depicted in Fig. 2.8 has the smallest surface area. A significant barrier in the LTO region is observed. Also for the HTO region, we see a steady increase in activation energy opposed to the previous case. This indicates that

the coke created is hard to burn because no plateau is reached. The LTO reaction identified before at $290°C$ (see Fig. 2.7) has shifted slightly to $303°C$ and activation energies have increased from $95KJ/mol$ to $140KJ/mol$.

Due to lack of sufficient reservoir core material for combustion tube runs a substitute had to be found. The *60 mesh sand/kaolinite combination* is an attempt to mimic the reservoir conditions. In terms of surface area, we are between the *16 mesh sand* and the *original reservoir matrix* case. The use of kaolinite added substantial complications in terms of experiments. With the kaolinite present, achieving a proper spread of the oxygen consumption curves was very difficult and several experiments failed. Trends for the isoconversional fingerprint observed are comparable to the production sand based experiment series but with some notable differences. First, reactions start at $\approx 190°C$ compared to $\approx 195°C$ for the production sand case and $\approx 205°C$ for the coarse sand case. Second, the reaction identified at $\approx 290°C$ for production sand and $\approx 303°C$ for the coarse sand example respectively has shifted to $\approx 320°C$. Third, the activation energy for the Death Valley was reduced significantly. Interestingly, the temperature difference between the humps in the LTO and HTO region is fairly constant ($\Delta T \approx 65°C$) regardless of the matrix used.

Relying on the isoconversional results as an indicator of whether or not a matrix/oil combination would burn successfully in a combustion tube, we made the following conclusions:

- The coarse 16 mesh sand matrix appears to be the least favorable candidate. Yielding comparably large activation energies in the LTO region ($\Delta E_a \approx 115kJ/mol$ with respect to Death Valley) and continuously increasing activation energy values for the HTO region make it unlikely for this combination to burn.

- The comparably unpronounced negative temperature gradient region for the kaolinite/sand combination and small activation energies for both LTO ($\Delta E_a \approx 33kJ/mol$ with respect to Death Valley) and HTO ($\Delta E_a \approx 58kJ/mol$ with respect to Death Valley) region combined with the smooth transition make it the most favorable candidate.

- The production sand experiment (without prior knowledge of the success of the

combustion process in the field) would be subject to discussion. The negative temperature gradient region is very pronounced and the humps in activation energy at the end of LTO ($\Delta E_a \approx 75kJ/mol$ with respect to Death Valley) and the beginning of the HTO ($\Delta E_a \approx 105kJ/mol$ with respect to Death Valley) region raise concerns.

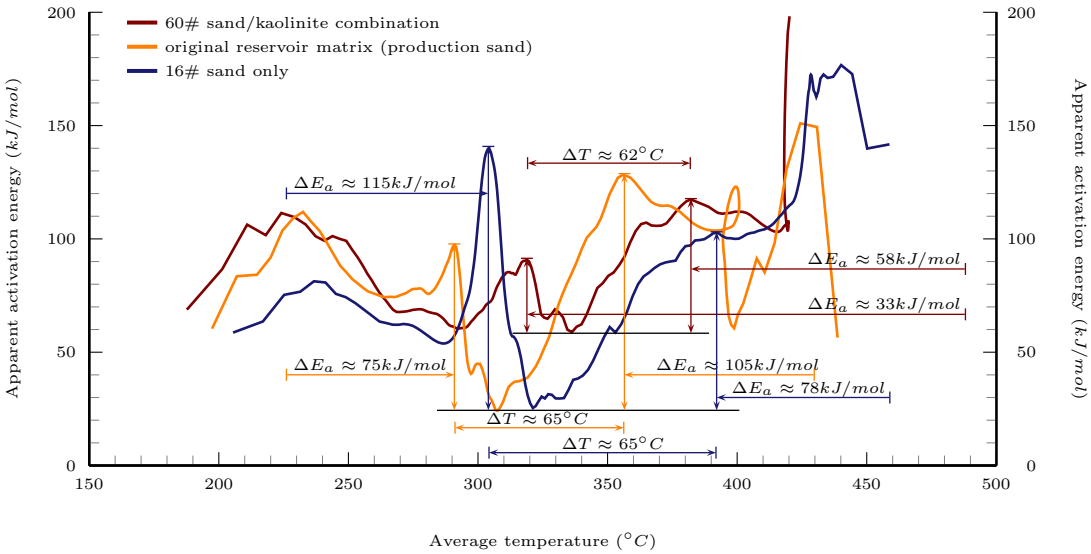

Figure 2.8: Summary of apparent activation energy for all solid/liquid mixtures.

Chapter 3

Combustion Tube Experiments

As pointed out in [43], combustion tube runs are not scaled experiments and act as a proxy for a differential element of a reservoir. When designing tube runs, heat losses are a major concern. The heat losses for tubes are due to the metal construction and cannot be compared with the heat losses resulting from the over- and underburden of the reservoir. In fact over- and underburden heat losses are generally small in comparison to experiments. Even after a combustion project has finished, the vast amount of heat stored in the reservoir is still observed after several years. To overcome heat losses, and prevent a premature termination of the combustion front, the tube was insulated using an aerogel based material.[1] Furthermore, the air flux is sufficiently large to sustain the combustion front.

3.1 Experimental Apparatus and Procedures

The combustion tube consisted of a thin-walled stainless steel tube measuring about 109 cm long × inner diameter 7.60 cm. Flanges were welded to both ends of the tube. On the inside of the bottom flange, interconnected, concentric grooves were machined to allow uniform flow at the bottom end of the tube. Each flange has a a knife edge machined onto its surface to provide a positive seal with a flat copper gasket. Thermowells were inserted through soldered Swagelock tube fittings at the

[1] `http://www.aerogel.com/`

top and bottom caps. Each thermowell consisted of 80 cm long stainless steel tube. A bundle of ten thermocouples soldered together with tips spaced at 2.5 cm intervals were placed in the thermowell making it possible to record temperatures at known positions in the tube. The tube fittings also allowed for gas injection and production respectively. A 40 mesh metal screen was secured at the tube fitting-plug assembly that sealed the bottom end of the larger thermowell. The combustion tube was sealed by a system of copper gaskets between the flanges, and twin ferrules at the thermowell-tube fitting connections. Heating for ignition purposes was achieved by a cartridge heater inserted through a fitting at the top flange and two band heaters wound around the tube some 10 cm below the top flange.

A typical combustion tube experiment was carried out as follows. Approximately 8000 g of sand and 150 g of kaolinite clay were placed in a plastic bin and mixed thoroughly by hand. Approximately 450 g of water was added to the sand-clay mixture. The mixture was thoroughly mixed until evenly moist. Approximately 450 g of crude oil was added and again mixed by hand until an even distribution of phases was achieved. This process takes between 60 and 80 minutes. With the bottom flange attached and the thermowell partially inserted, the tube was securely fastened in a vertical position. Small portions of the sample were introduced into the tube. Using a metal plunger, the sample was tamped heavily into the tube. After adding about 3 samples and plunging them, the bottom thermowell was carefully inserted to a point where the tip of the thermowell could still not be seen from the top. This process of adding sample, subsequent tamping and inserting of the thermowell was repeated until the thermowell was fully inserted in the tube (about 2/3 of the tube length). This procedure guaranteed a very tight and dense packing. For the remaining part of the tube, the introduced samples could not be tamped as heavily as the lower part. The thermocouple had to be inserted after the top flange was secured making it very difficult, if not impossible, to insert the top thermocouple when packed tightly.

After tightening all connections and attaching the sampling system at the bottom of the tube, the tube was tested for leaks. Nitrogen, was introduced at the injection inlet at the top of the combustion tube. With the outlet of the combustion tube plugged, the tube was pressure tested to approximately 170 psig and checked for

leaks. After depressurizing, the tube was insulated as described in [30].

Overnight the tube was stored in a horizontal position to reduce gravity drainage effects. The next day the tube was secured in a vertical position, all tubes and sensors were hooked up, the gas analyzer calibrated and nitrogen injection started. The gas injection rate was set on the mass flow controller at approximately 2 l/min. The back-pressure regulator was adjusted to obtain an injection pressure of about 100 psig. Electric current was introduced into the heater cartridge and the band heaters in gradual steps using a variable power transformer. When the temperature in the combustion tube at the heater thermocouple reached approximately 500 $°C$, air injection was initiated and the power to the heating devices was gradually reduced over a time frame of 30 to 45 minutes. The air injection rate was set to 3 l/min. During most of the experiments the back-pressure regulator was adjusted for an injection pressure of 100 psig to obtain reservoir conditions. In some special cases the pressure was not adjusted. The pressure of the tube, exit flow rate, temperature, and effluent gas composition were recorded continuously during the experiment.

Typically right after air injection began, a dramatic rise in temperature was observed. For most cases water production started after 2.5 hours, whereas oil production started after 4 hours after ignition. Produced liquids were collected in the sample system. Due to the initially undersized sampling system, the liquids had to be collected from the sampling bomb into graduated sample bottles that were tightly capped for subsequent analysis. For safety reasons the sand pack was was not burned to the bottom flange and combustion was stopped about 25 cm above the bottom flange by flushing the tube with nitrogen at a flow rate of 3 l/min. A typical run required between 4 to 6 hours of air injection depending on flow rate. Overnight, the tube was left in a vertical position to let oil drain and for cooling.

The next day, the setup was dismantled and a post mortem analysis was performed. During the post mortem analysis the remains of the sand pack were collected, categorized, and weighed. This helped to provide information on the axial profile in terms of coke, water, and extractable oil.

3.2 Experimental Data Collected

Physical data obtained automatically from combustion tube runs are as follows:

- Effluent CO_2, CO, CH_4 and O_2 concentration.
- Temperature measurements from along the tube, 20 individual measurements in total.

As in the case of the kinetic cell, data are not used directly. Again care has to be taken for the lag introduced by the gas analyzer, as well as the lag between temperature readings and gas measurements. Fig. 3.1 and Fig. 3.2 show the the gas and temperature readings of the first combustion tube run. The matrix and liquid composition used in this case is summarized in Table A.6. In terms of composition this setup corresponds to the kinetic cell run using fine sand and clay (see Fig. 2.8 for activation energies and Table A.5 for oil, water, sand, and clay proportions).

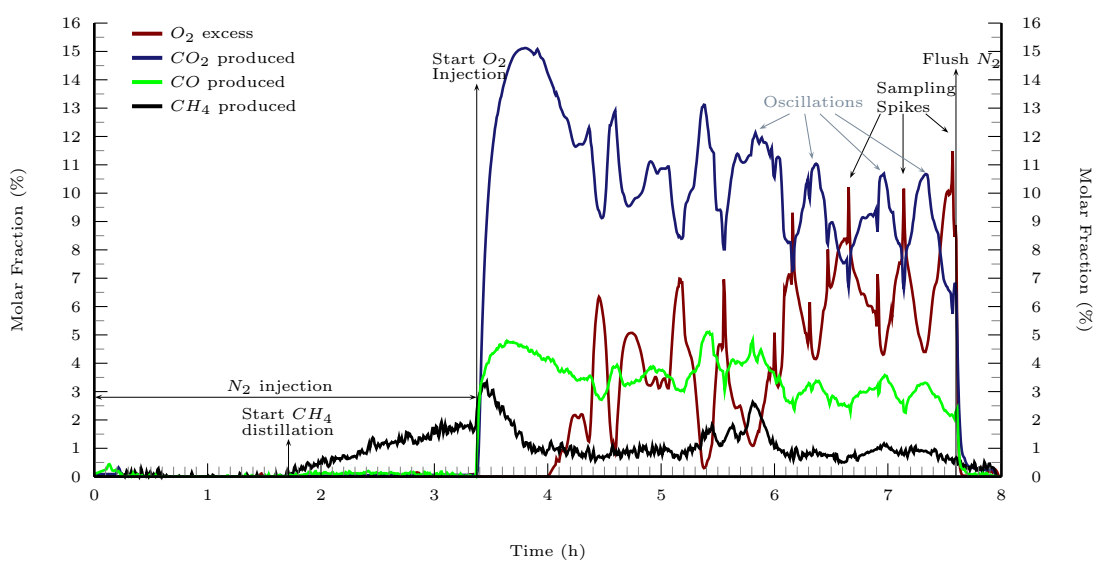

Figure 3.1: Gas measurements for RUN 1.

The combustion tube run is started by gradually increasing the temperature of the heater to $\approx 500°C$. This corresponds to the time from $0 - 3.5$ hours in Fig. 3.1 and Fig. 3.2 respectively. During that time, nitrogen is injected to prevent premature

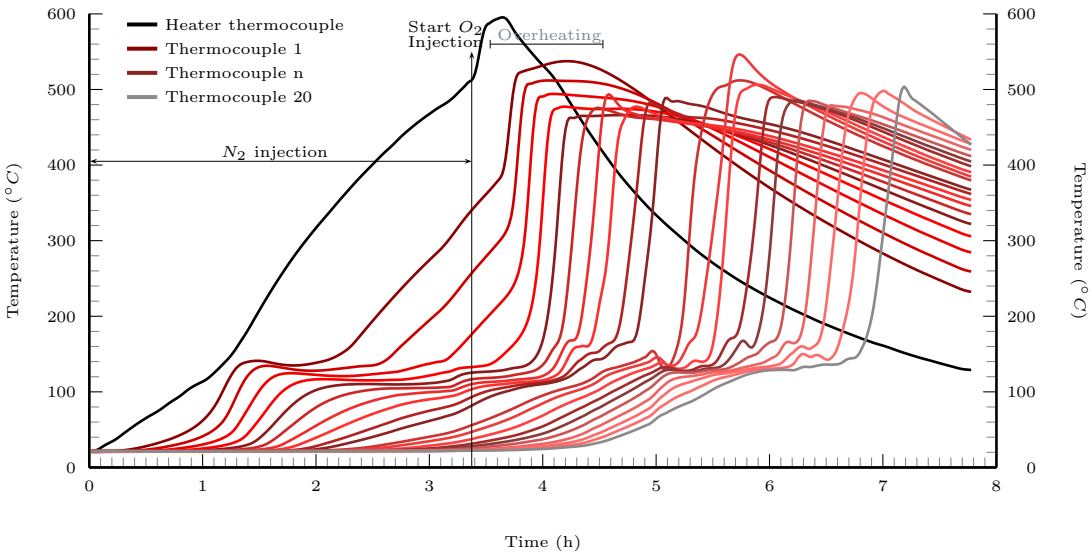

Figure 3.2: Temperature profile for RUN 1.

ignition. 1.7 hours into the experiment a high enough temperature is reached allowing CH_4 to be released from the oil. After 3.5 hours, we switched from nitrogen to air. Accordingly, we saw a rapid increase in gas production as well as in temperature. Due to inexperience with this particular crude oil, the heater was not switched off immediately to ensure proper ignition. Eventually heaters were switched off 4 hours into the experiment. This resulted in overheating as is seen in Fig. 3.2 from $3.5 - 4.5$ hours. For all other experiments, heaters were gradually decreased within a thirty to fourty minute time frame after ignition. Once ignition was successful, the experiment was allowed to continue until the combustion front reached the lower quarter of the tube (≈ 7.65 hours into the experiment). Finally, the tube was flushed using nitrogen to extinguish the combustion front.

Examining the gas production shown in Fig. 3.1, between $3.5 - 6$ hours into the experiment gas readings seem rather chaotic. No relation between oxygen consumption and flue gas production is apparent. We have to keep in mind that during this time the combustion front is moving through a loosely packed part of the the tube. From $6.0 - 7.65$ hours a more harmonic behavior is seen manifesting itself in form of more or less constant oscillations. During this time, sharp spikes are observed in oxygen consumption and - to a lesser extent - in flue gas production. These spikes

are a direct result from the sampling process. For most combustion tube runs, the volume of the sampling bomb was not large enough to hold all liquids produced. The sampling bomb, therefore, had to be emptied from time to time. In order to do this, the bottom of the tube had to be shut-in to enable safe sampling. During sampling, the pressure increased from the operating pressure of 100 *psi* to about 130-160 *psi* depending on the time needed for sampling. When the valve is opened again, the pressure drops back to the original operating pressure and air flushes the previously emptied volume of the sampling bomb. This causes a temporary increase in oxygen consumption and, subsequently, flue gas production. As a side effect this causes destabilization of the current gas reading and the harmonic oscillation is partly masked. Using the Savitzky-Golay filter, these oscillations were removed in Fig. 3.3. Selecting the filter properties carefully, the shape of the original signal is preserved. Not only did this help us to better identify any relations between individual gas readings. We also get better data for future simulation. The filtering technique was applied for all following gas production figures.

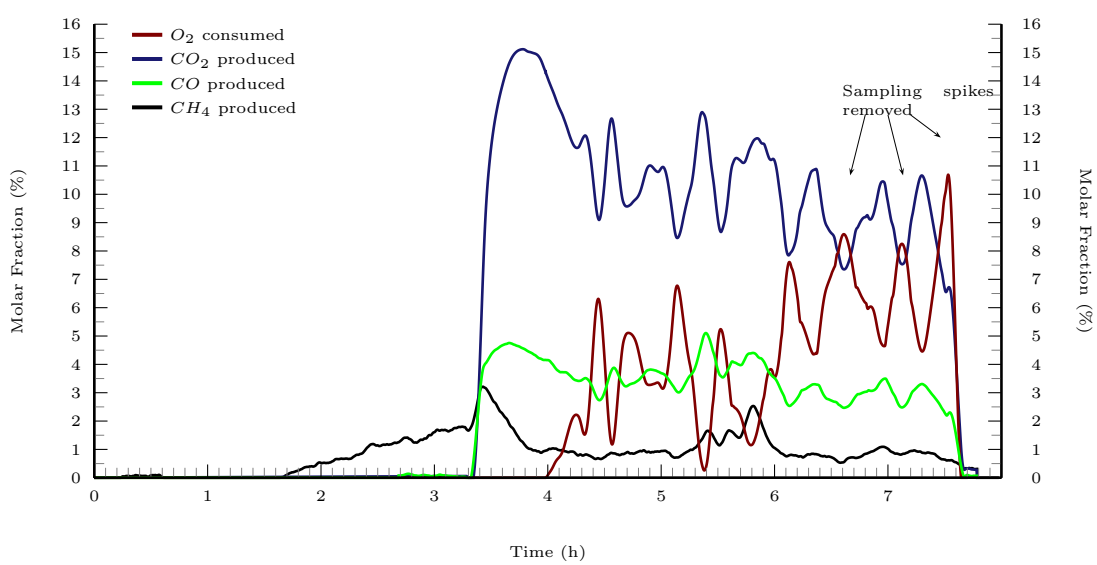

Figure 3.3: Filtered gas data for RUN 1.

In Fig. 3.2 we can see that the temperature of the combustion front is between 460 $°C$ and 520 $°C$. The first temperature profile (colored black) corresponds to the heater thermocouple and gives an idea of the heating profile applied. Furthermore,

we can clearly see the steam plateau around 110°C during the initial response of each thermocouple. The temperature for the steam plateau is not constant because we have to take changing partial pressures into account. Also the sampling process, as described above, allows for a temporary pressure change. Based on the temperature profile the average velocity of the combustion front was calculated. Taking only the maximum temperature readings for the well packed region into account we calculated the velocity knowing the spacing between the individual thermocouples. Using linear regression (see Fig. 3.4) an average velocity of 13.5 cm/h was obtained.

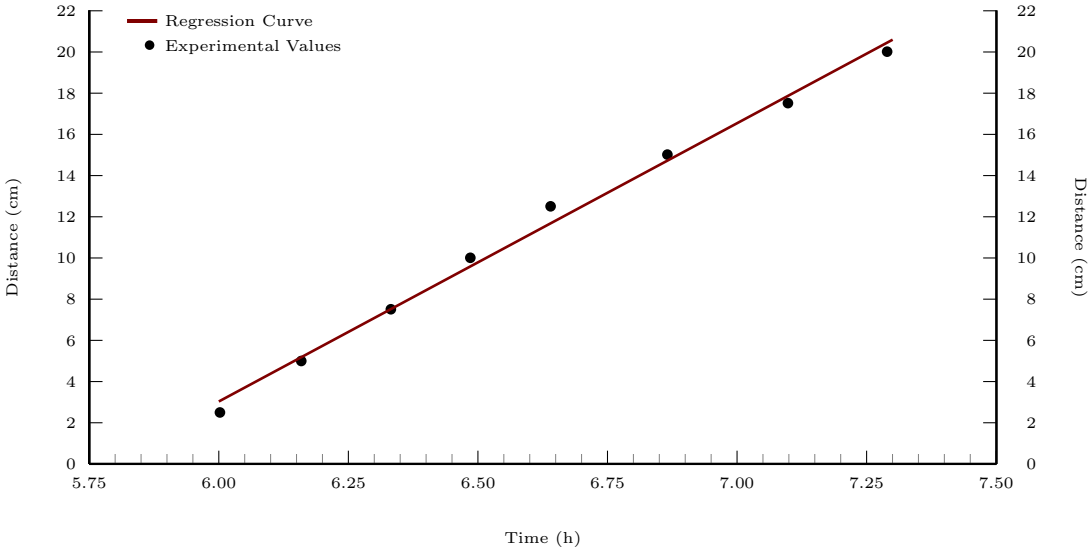

Figure 3.4: Determination of combustion front velocity for RUN 1.

Heating rates were calculated based on time needed for the temperature increase from 200 °C to 400 °C. For RUN 1, heating rates range from 25 °C/min to 30 °C/min. Notably, combustion tube heating rates in this case are a factor of 10 greater than heating rates used in kinetic cell experiments ($\approx 2°C/min$). Heating rates in the reservoir, however, are believed to be in the range of kinetic cell heating rates [22].

3.3 Production Data and Post Mortem

The basic mixture used for a combustion tube run consisted of sand, powdered kaolinite, water and oil (see Table A.6). The actual reservoir properties could not be matched quantitatively for several reasons. First, an assumed initial oil saturation of 85% would have overloaded the production vessel. Second, at the time the combustion tube runs were carried out, no general consensus about the amount and type of clay existed (see Table A.3). Given that all kinetic cell runs were made using kaolinite, it was decided to continue using this type of clay to mimic an increased surface area and account for any catalytic effect. In order to make tube runs comparable with tube runs from previous studies the range for clay in terms of weight percent was set to a range of [1.8-2.0], the range for oil and water was set to a range of [5.0-6.0].

Water production started between two and four hours after ignition. The production vessel had no window so it was not possible to determine the exact start of water production. As mentioned above during the sampling process, the tube was shut-in and water and/or oil was released. This continuous sampling process proved to have several disadvantages. Due to the great pressure drop, liquids could easily be spilled or evaporated. Also the constant opening and closing of the production vessel fostered the movement of fines, ending up in the production part of the assembly. This is also one of the reasons why values in Table A.6 do not add up exactly with production data and weighing results of post mortem analysis. Total production data as shown in Table A.13 does not give absolute values. It serves as an accurate estimate of actual production data.

After the tube was cooled down - usually after 15 to 17 hours - the post mortem analysis was performed (see Fig. 3.5). During the post mortem analysis the tube content was examined. This included dividing the remains in several zones and measuring the respective weight (see Table A.17). Starting from the top of the tube (heater position) the first zone is referred to as pyrolysis coke. This coke was created in the absence of oxygen in a nitrogen environment during the heating up process. This coke has very large activation energies because not all of it gets burned. Below the pyrolysis coke a very clean burned zone is found, usually referred to as *Burned*

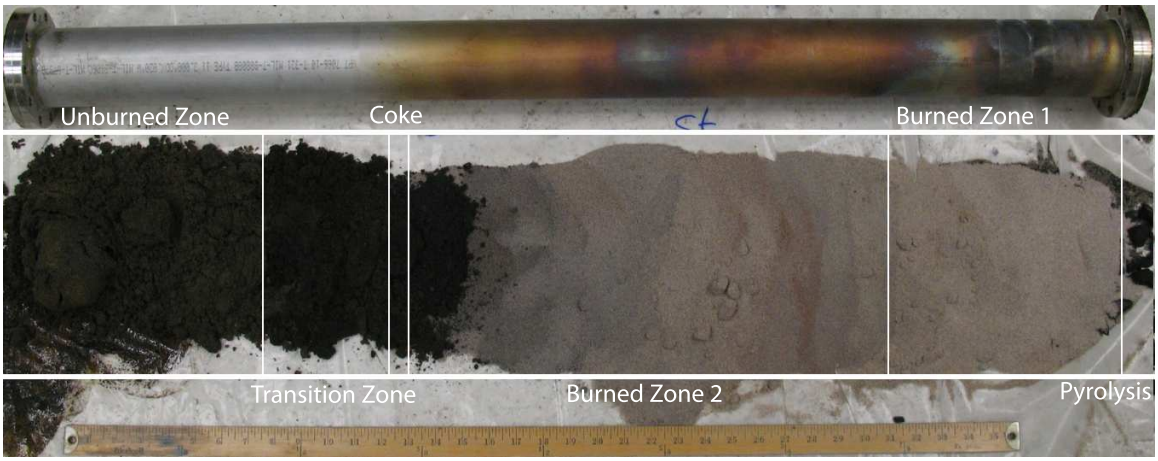

Figure 3.5: Post mortem for RUN 1 (weighing results given in Table A.17).

Figure 3.6: Coke residue for Run 1 (thickness is ≈ 1 inch).

Zone 1. Below *Burned Zone 1*, *Burned Zone 2* is found. There are two main reasons why *Burned Zone 1* is cleaner (or lighter visually speaking). First, this zone was subject to the heater cartridge and the band heaters. Therefore, more energy was available once the tube was ignited and the burning process was more complete. Second, the upper part of the tube was less compacted for reasons mentioned in the previous section. For all runs, the observation could be made that the burned zone in the well packed part of the tube was darker than the burned zone in the not so well packed part of the tube. This is easy to understand because apparently more oil was available in the lower part of the tube. Also, it can be assumed that the permeability of the upper part of the tube is greater compared to the permeability of the lower part of the tube. Again, and indicator that for a successful field run, the reservoir permeability has to be reasonably high.

The next zone represents a snapshot of the combustion front where HTO reactions took place. It has to be kept in mind though, that this is not how the real combustion front appears. Once the tube run was finished and nitrogen injection was commenced cracking reactions etc. are still going on because the tube cannot be cooled down instantly. The thickness of the coke ranged from 0.5 to 2 inches (see Fig. 3.6). The next zone was a transition zone were cracking and LTO reactions started to take place. Finally, we have the unburned zone which basically represents the oil bank.

3.4 Stoichiometry

According to [4], the combustion stoichiometry for HTO is expressed as:

$$\begin{aligned} &CH_n + \frac{1}{Y}\left(\frac{2m+1}{2m+2} + \frac{n}{4}\right) O_2 + \frac{R}{Y}\left(\frac{2m+1}{2m+2} + \frac{n}{4}\right) N_2 \rightarrow \\ &\frac{m}{m+1} CO_2 + \frac{1}{m+1} CO + \frac{1-Y}{Y}\left(\frac{2m+1}{2m+2} + \frac{n}{4}\right) O_2 \\ &+ \frac{n}{2} H_2O + \frac{R}{Y}\left(\frac{2m+1}{2m+2} + \frac{n}{4}\right) N_2 \end{aligned} \tag{3.1}$$

The stoichiometric coefficients can be calculated based on normalized gas composition

i.e. taking only O_2, CO_2, and CO of effluent gas analysis into account [8, 48]. In Eq. 3.1, m is the molar ratio of CO over CO_2 and R is referred to as the ratio of the mole fraction of nitrogen to oxygen in the feed gas i.e.

$$R = \left(\frac{Y_{N_2}}{Y_{O_2}}\right)_{Feed\ Gas} \tag{3.2}$$

n stands for the equivalent atomic H/C ratio of the fuel burned. It is important to point out, that the H/C Ratio only characterizes the HTO reactions. It does not represent the composition of the fuel actually burned in the combustion tube because of the LTO reactions that occur in the tube at temperatures below $350°C$ [44]. The effluent gas measured is a result of both LTO and HTO reactions. In terms of normalized gas composition, n is given with

$$n = \frac{4\left(\frac{N_2}{R} - CO_2 - \frac{CO_2}{2} - O_2\right)}{CO_2 + CO} \tag{3.3}$$

Based on effluent gas data from RUN 1 and using average values for the stabilized region, the following stoichiometry for the HTO reaction was obtained:

$$\begin{aligned} &CH_{1.25} + 1.48O_2 + 5.67N_2 \ \rightarrow \\ &0.75CO_2 + 0.25CO + 0.29O_2 + 0.63H_2O + 5.67N_2 \end{aligned} \tag{3.4}$$

Given that the H/C ratio of the original oil is estimated to be 1.7 and the H/C ratio of the fuel is 1.25 we conclude from the H/C ratio reduction, that high temperature oxidation was the main oxidation mechanism i.e. most of the oxidation reactions happened in the HTO region [48]. Butler and Sarathi list several other important parameters commonly referred to as gas-phase parameters. Among them is the oxygen-fuel ratio (OFR) that is described as the minimum volume of oxygen required to burn a unit mass of fuel that has an equivalent atomic H/C ratio given

by n. The OFR is believed to be directly proportional to the degree of LTO occurring in the combustion tube. As mentioned above, during LTO some fraction of the consumed oxygen reacts with the crude oil without generating any of the carbon oxides or water. The air-fuel ratio (AFR) refers to the volume of air required to burn a unit mass of fuel. It is of great value when designing a field project. During a combustion tube run some fraction of the consumed oxygen reacts with oil to form oxygenated compounds commonly referred to as f_{O_2R}. This is especially true for LTO. According to [48] calculating the fraction of reacted oxygen converted to carbon dioxides gives an idea to which extent LTO reactions occur in the combustion tube. The results for RUN 1 (and all other runs) in terms of gas phase parameters for the stabilized region based on mean values are summarized in Table A.16.

In addition to calculating single values for the stabilized region it is also very helpful to calculate the individual gas phase parameters for each gas reading. In Fig. 3.7, O_2, CO_2, m, H/C ratio, and f_{O_2R} are compiled into a single plot. As we can see, HTO reactions dominate over the entire tube run because the H/C Ratio is below the H/C ratio of the original oil i.e. 1.7. We also see that m starts to level out around 3 for the stabilized region.

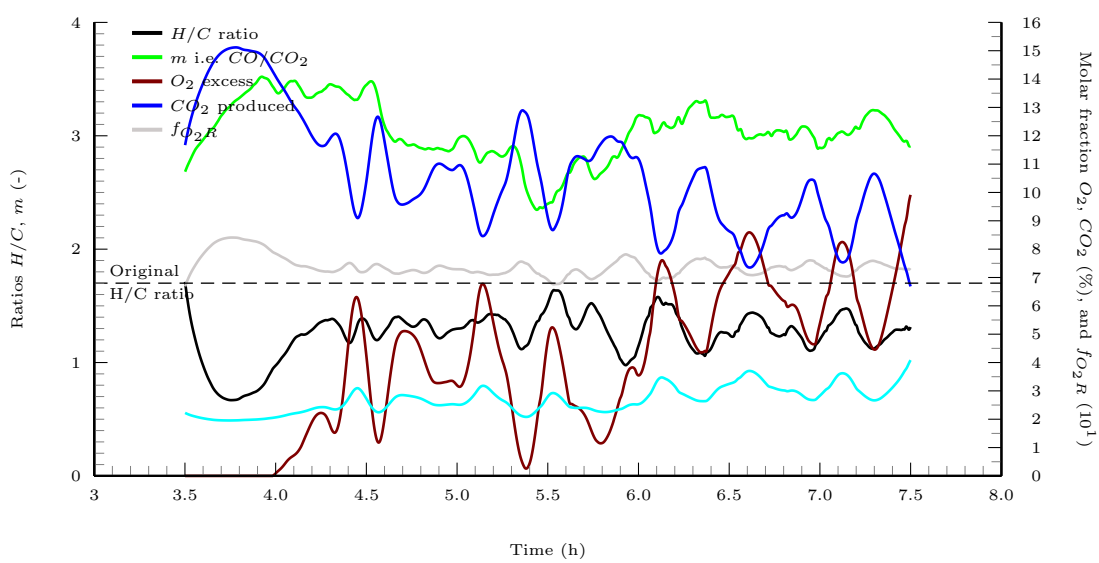

Figure 3.7: Selected parameters for entire experiment, RUN 1.

Comparing the H/C ratio over time with measured O_2 data, we find that in times

of less oxygen consumption a comparably larger H/C ratio is observed. Given that f_{O_2R} is an indicator to the extent which LTO reactions occur in the combustion tube, it appears, that a greater H/C ratio also corresponds with a greater amount of LTO reactions. This periodic change from less oxygen consumption, greater H/C ratio, and smaller f_{O_2R}, to greater oxygen consumption, smaller H/C ratio, and greater f_{O_2R} is especially true for the stabilized region. These oscillations have been mainly attributed to geomechanical i.e. packing issues, meaning bulk density differences arising from the packing procedure used for combustion tube preparation [30]. In this case, however, oscillations cannot be attributed solely to packing issues. This is particularly true for the lower part of the combustion tube. The packing procedure described above guarantees a homogeneous medium to a great extent. In order to blame packing for oscillations the frequency of the oscillations has to be related physically to the packing process.

Let us assume the following. Filling a combustion tube takes roughly 90 scoops of sample, each scoop weighing about 100 g. Each scoop is consolidated using a metal plunger. Accordingly, 90 layers of different density are created. Each layer being about 1.2 cm thick. This is what is referred to as inhomogeneous packing. Given that the combustion front moves at a velocity of 13.5 cm/h, the front passes around eleven different layers in one hour. If each layer gives a peak the distance between the amplitudes is about 1.2 cm which equals to half a period. Consequently it takes the combustion front 0.18 h to travel a full period. The resulting frequency of the signal is then around 5.6 Hz. The frequency of the oscillations for the unstabilized zone from 4.5 to 6 hours in Fig 3.7 is around $7.9 \times 10^{-4}\ Hz$. For the stabilized zone (from 6 to 7.5 hours), it is even less with $5.6 \times 10^{-4}\ Hz$ and remarkably constant (compare with RUN 2). To conclude, the frequency observed is too low to be related to packing.

A more general explanation could be as follows. Looking at Fig. 3.22 on page 43 the amplitude of the oscillations seems to be affected by the flow rate. The lower the flow rate (see Fig. 3.20), the lower the amplitude of the oscillations. Also, the lower the flow rate, the lower the frequency of the oscillations. As mentioned before, a maximum in excess O_2 corresponds to a minimum in CO_2 production and vice versa.

The same is true when comparing O_2 and CO readings. In Fig. 3.7, it appears, that a maximum in O_2 also is accompanied by a maximum in H/C ratio and a minimum in f_{O_2R}. If we once again assume that the apparent H/C ratio describes the type of fuel we burn (with the limitations mentioned on page 26), we deduce that an oxygen rich environment leads to a fuel having a greater H/C ratio. This conclusion is also supported by the fact that if excess oxygen is greater, less heat is released that directly affects the cracking process etc. Adversely, fuel created in an oxygen deficient environment (more heat released) results in a small H/C ratio. Due to the large heating rates we can assume that the combustion front and the place where the coke is created ahead of the front are close together. Based on average heating rates for RUN 1 (see page 22) and kinetic cell results the coke creation zone is less than 6 to 9 minutes ahead of the combustion front. Given an average velocity of the combustion tube front of 13.5 cm/h the coke is created between 1.35 and 2.03 cm ahead of the front. A small H/C ratio indicates a large carbon content. From kinetic cell runs we know, that coke created in a nitrogen environment (i.e. oxygen deficient environment) burns at comparably higher temperature and in a smaller temperature window. Coke created under oxygen starts burning at lower temperatures over a wider temperature range.[2] Consequently if the H/C ratio decreases, and the fuel becomes more carbon rich, higher temperatures are needed to burn the fuel. If ignited, though, substantially more oxygen is consumed leaving less oxygen available in the zone where the coke is created. As the fuel is created in a more and more oxygen deficient environment the H/C ratio decreases and even higher temperatures are needed to ignite the fuel. At a certain point, the fuel reaches a H/C ratio limit a self-sustaining process can burn for a given temperature. Consequently, less oxygen is used in burning reactions and becomes available for the coke formation process ahead of the front. The coke created in the oxygen rich environment is considered more reactive[3] and starts burning at lower temperatures. Oxygen consumption starts increasing again leaving less and less oxygen available for coke generation ahead of the front. The overall result is a oscillating process seeking equilibrium between coke created and oxygen availability.

[2]Personal Communication with M. Cinar.
[3]Personal Communication with M. Cinar.

Therefore, when oxygen flow rate is just enough to sustain the front, and coke is always created in an oxygen deficient environment, oscillations should disappear. This behavior was observed for RUN 7 (see Fig. 3.22). In addition, for RUN 7 the pressure was not adjusted. From the sampling process it is known that a change in pressure also affects gas concentrations. An additional effect of pressure changes cannot be ruled out.

3.5 Operational Data

Calculating operational data as summarized in Table A.15, the entire tube run was taken into account. Values represent only rough estimates and are based on the assumption that inlet and outlet flow rate are the same. Oil recovery is based on the volume swept which is basically comprised of *Burned Zone 1* and *Burned Zone 2*.

3.6 Repeatability

If we use stoichiometry as calculated previously, we obtain a certain value for CO_2 and CO for a given value of O_2. In a simulation we will not be able to achieve completely the same results because we cannot model preparation of the mixture, the packing process etc. We should be, however, able to obtain the the same CO_2 and CO values for a given value of O_2. Plotting the CO_2 and CO versus O_2 gives an idea, of the range of values. The range will be a function of mixture, packing, stoichiometry, and operating conditions. This helps to verify the simulation model. Furthermore, it is a simple yet helpful consistency check.

In Fig. 3.8 we can see, that there is a linear relation between excess oxygen and flue gas production. If all oxygen is consumed, we can expect a CO_2 mole fraction of 13.54% (with 95% confidence bounds of [13.47 13.61]) and a CO mole fraction of 4.44% (with 95% confidence bounds of [4.40 4.8]). Given the narrow range for the mole fractions, we conclude that the experiment was conducted in a consistent manner.

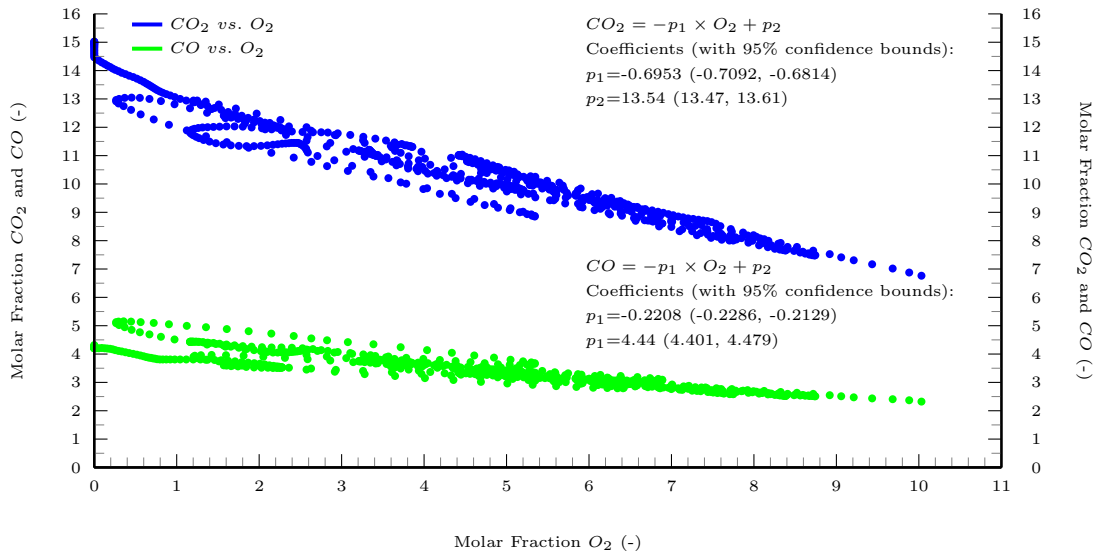

Figure 3.8: CO_2 and CO as a function of excess O_2 for RUN 1.

3.7 Individual Combustion Tube Results

3.7.1 RUN 1

All experimental results for RUN 1 were used to describe the post-processing steps above. Gas phase parameters and operational data is summarized in Table A.16 and Table A.15 respectively. Production data is given in Table A.7.

3.7.2 RUN 2

RUN 2 served as a control experiment for RUN 1. Basically the same experimental setup was used (see Table A.6 for sample mixtures). Again air flow rate was 3 l/min and pressure was held constant at 100 psi. For the stabilized zone a velocity of 13.9 cm/h is obtained.[4]

The only difference in terms of operational conditions was, that the heaters were shut-off 25 minutes after ignition minimizing the artificial energy added to the system (compare Fig. 3.9 with Fig. 3.2). In terms of gas production data, CH_4 production was more stable (compare time frame from 5 to 6 hours). In both cases CH_4 started

[4]With 95 % confidence bounds: [13.4 14.4] cm/h. Velocity for stabilized region for RUN 1 was 13.5 cm/h (with 95 % confidence bounds: [12.4 14.6] cm/h).

to be produced when the heater reached about 200°C. For RUN 1, the combustion front stabilized at about 490°C whereas for RUN 2 the combustion front stabilized at about 450°C. The difference could be a result of the different heating programs applied.

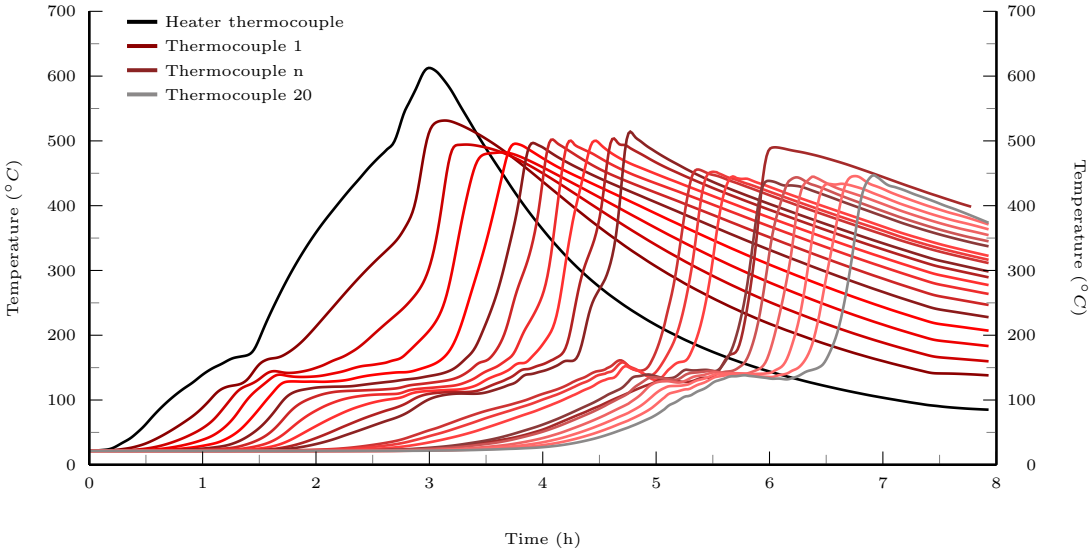

Figure 3.9: Temperature profile for RUN 2.

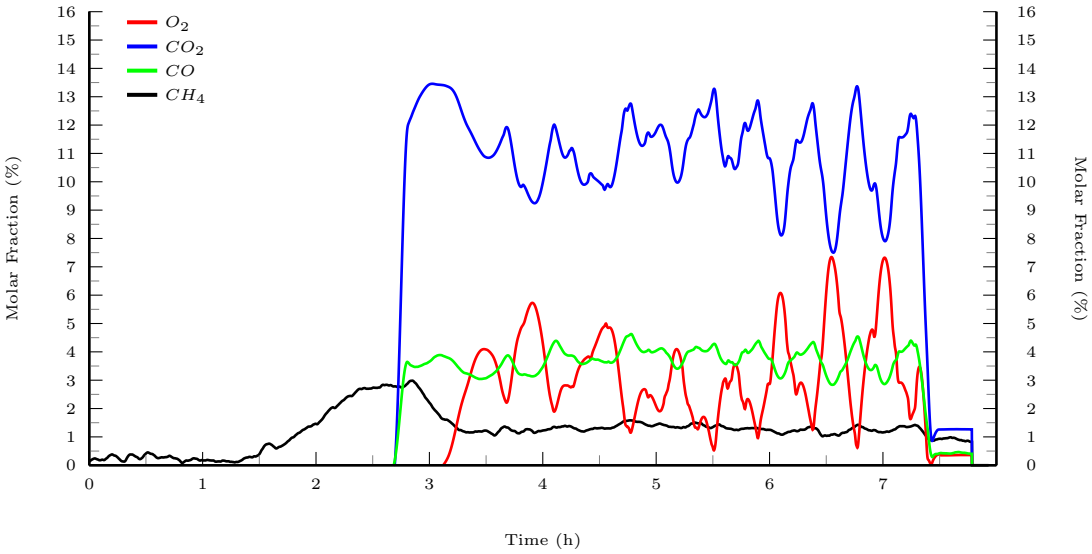

Figure 3.10: Gas data for RUN 2.

Cumulative production data is given in Table A.8. Operational data is summarized

in Table A.15. The overall H/C Ratio is the same compared to RUN 1. In RUN 2, though, more fuel was consumed (23.2 kg/m^3 versus 18.8 kg/m^3) resulting in comparably higher air requirements (291 $m^3(ST)/m^3$ versus 248 $m^3(ST)/m^3$).

The result of the post mortem analysis is summarized in Table A.17. For RUN 2 almost twice the amount of pyrolysis coke was obtained. This is understandable because heaters were turned off considerably earlier compared to RUN 1. Less artificial heat was, therefore, available to burn this type of coke. In terms of stoichiometry for the stabilized region, however, both runs are the same (compare Eq. 3.5 with Eq. 3.4).[5] In either case the same fuel is burned and both runs suggest that HTO reactions dominate.

$$\begin{aligned} &CH_{1.26} + 1.41O_2 + 5.41N_2 \rightarrow \\ &0.74CO_2 + 0.26CO + 0.23O_2 + 0.63H_2O + 5.41N_2 \end{aligned} \tag{3.5}$$

The same is true to a great extent for gas phase parameters (see Table A.16). Fig. 3.11 shows selected parameters for the entire experiment (compare with Fig. 3.8). In the oxygen consumption curve we can see artifacts from the sampling spike removal process (e.g. 6.8 hours into the experiment, positive flank of the oxygen consumption curve). As mentioned above, during each sampling process the tube is shut-in for half a minute and then opened again. This causes air to flush through the tube and fill the previously emptied sample bomb volume. The air flush causes the combustion front to increase in temperature momentarily and the coke created ahead will be less hydrogen rich. As a result we can see a subsequent drop in H/C ratio. Once the lower H/C ratio fuel is burned, the previous trend continues.

[5] We have to keep in mind that calculating operational data is subject to personal interpretation e.g. defining zones during the post mortem. Comparing stoichiometry is more objective.

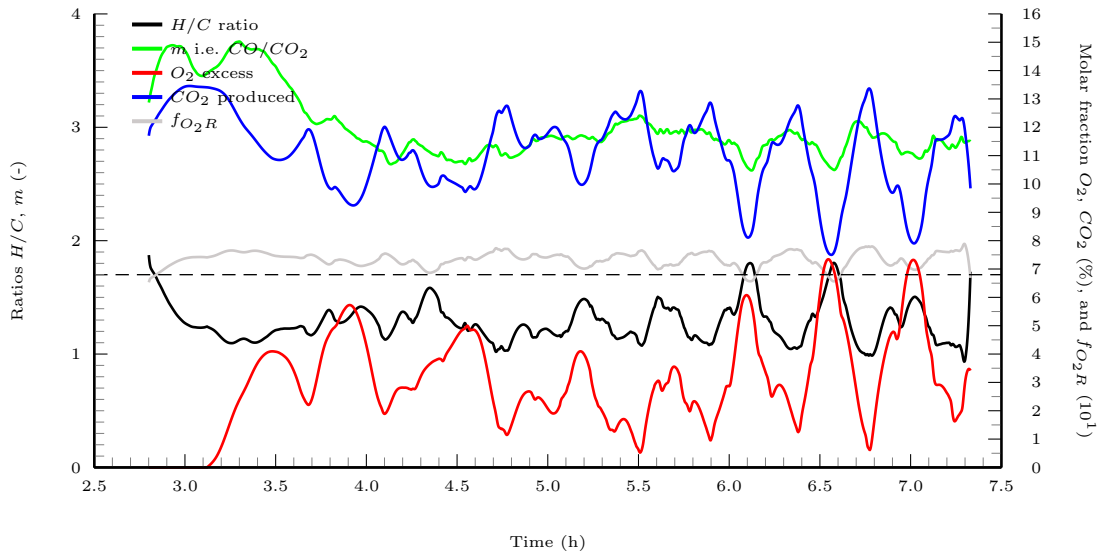

Figure 3.11: Selected parameters for the entire experiment, RUN 2.

3.7.3 RUN 3

The third run was carried using oil from a different well. The sample mixture (see Table A.6) and operational conditions are comparable with RUN 1 and RUN 2 respectively. For the stabilized zone a velocity of 15.4 cm/h is obtained (with 95 % confidence bounds: [14.1 16.8] cm/h). Gas production data is given in Fig. 3.12 and temperature profiles are given in Fig. 3.13. Comparing the temperature profiles of RUN 3 with profiles of other RUNS several issues can be observed. In Fig. 3.13 the heater thermocouple gives temperature spikes between 5 and 6 hours into the run. These spikes are a result of faulty readings by the heater thermocouple.

Also temperature readings for the well packed zone were skewed in nature. The reason for this is still unknown. Compared to RUN 1 and RUN 2 ignition for RUN 3 was much more pronounced (compare Fig. 3.13 with Fig. 3.9 and Fig 3.2 respectively).

The temperature stability problems are also reflected in the stoichiometry. RUN 3 was the only run having a H/C ratio above 1.7 (see Eq. 3.6 and Table A.16 respectively) for the stabilized region.

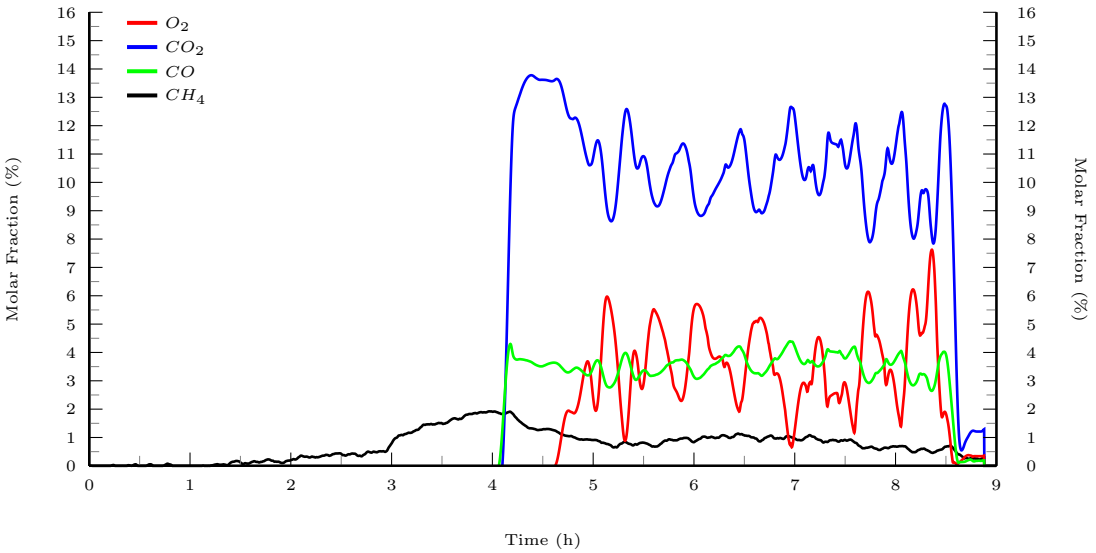

Figure 3.12: Gas data for RUN 3, Well 2360.

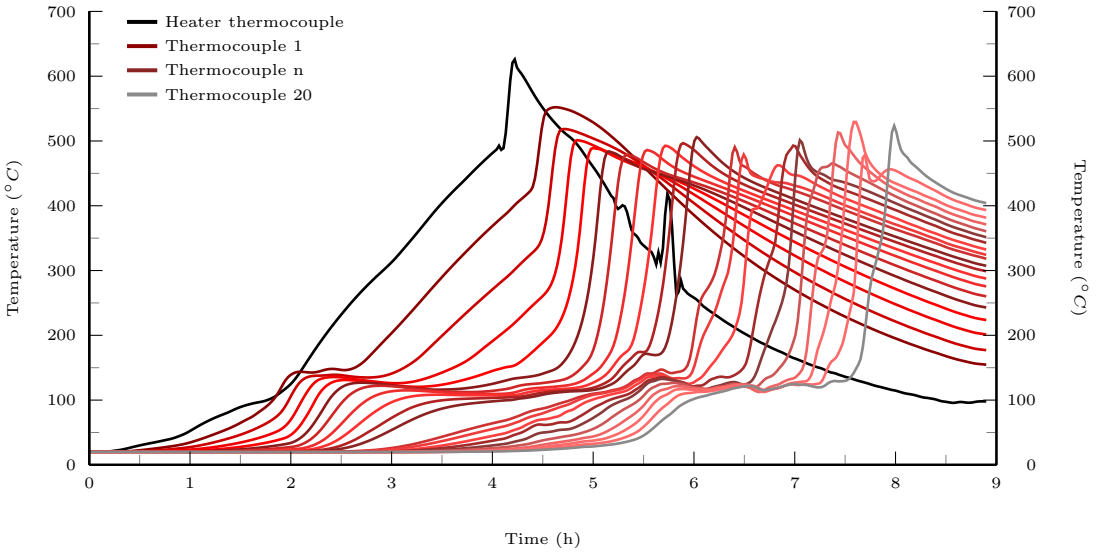

Figure 3.13: Temperature Profile for RUN 3.

$$CH_{1.86} + 2.65O_2 + 5.97N_2 \rightarrow$$
$$0.75CO_2 + 0.25CO + 0.25O_2 + 0.93H_2O + 5.97N_2 \quad (3.6)$$

Considering the entire run, however, H/C ratio was at 1.45 (see Table A.15).

3.7.4 RUN 4

RUN 4 served as a control experiment for RUN 3. The same experimental setup was used (see Table A.6 for the sample mixture). Again air flow rate was 3 l/min and pressure was held constant at 100 *psi*. For the stabilized zone, a velocity of 15.4 cm/h is obtained (with 95 % confidence bounds: [14.2 16.6] cm/h). Gas production data (see Fig. 3.14) is basically the same as for RUN 3 (see Fig. 3.12). For RUN 4 stabilization could be reached very early. Partial destabilization in gas production data resulted from sampling. Also temperature profiles are the same. Again, when the combustion front hit the well packed zone initial temperature profiles got skewed (see Fig. 3.15). In terms products, stoichiometry of RUN 4 (see Eq. 3.7) and RUN 3 (see Eq. 3.6) give comparable results. Concerning reactants RUN 4 has a significant lower H/C ratio (see Table A.16).

$$CH_{1.37} + 1.41O_2 + 5.42N_2 \rightarrow$$
$$0.74CO_2 + 0.26CO + 0.20O_2 + 0.69H_2O + 5.42N_2 \quad (3.7)$$

The fact, that the same experimental conditions can yield different H/C ratios point out the importance of control experiments. In terms of operational data (see Table A.15) the second highest oil recovery was obtained.

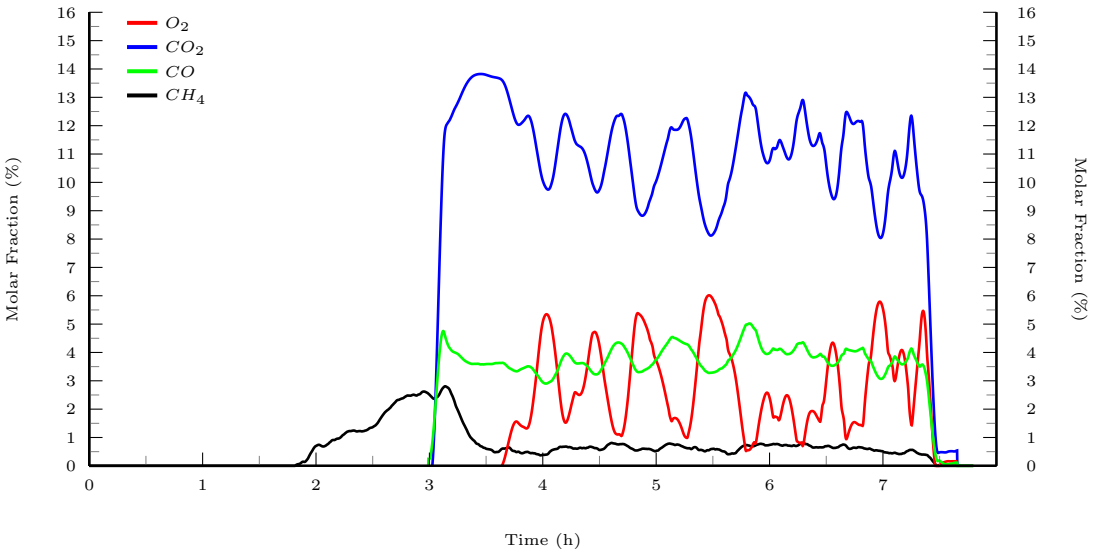

Figure 3.14: Gas data for RUN 4.

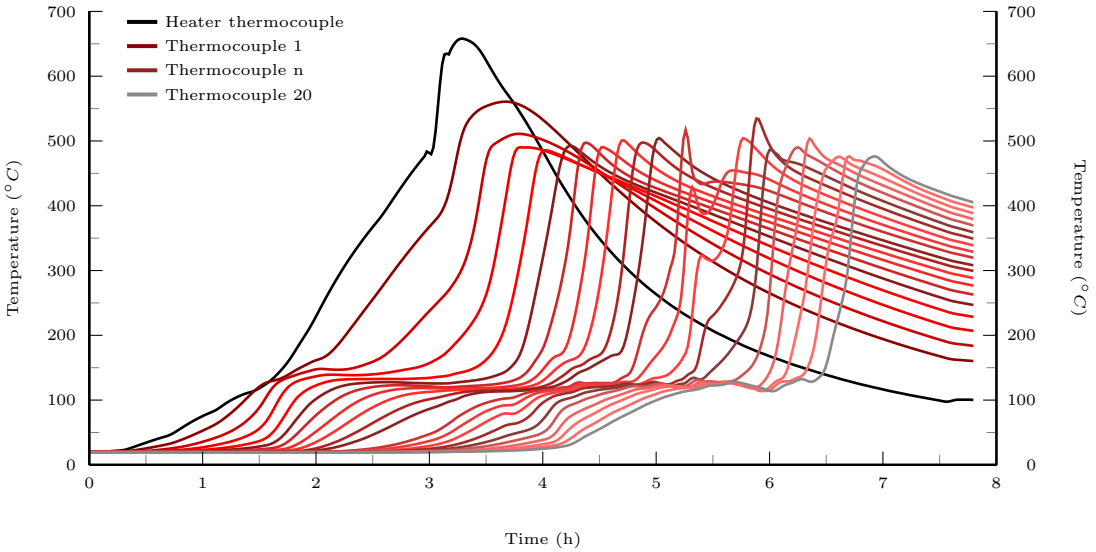

Figure 3.15: Temperature Profile for RUN 4.

3.7.5 RUN 5

The main purpose of *RUN 5* was to investigate the effect of reduced surface area on ISC. Instead of 60# sand a 16# sand was used (see table A.6).[6] All other operating parameters were kept the same.

Shortly after the start of the experiment the flow line connecting the air supply to the top of the tube broke off and all gas was bled off (see Fig. 3.16 and Fig. 3.17, between 3.5 and 4 hours into the experiment). The connection line was repaired and reattached within a couple of minutes and the combustion front could be reignited.

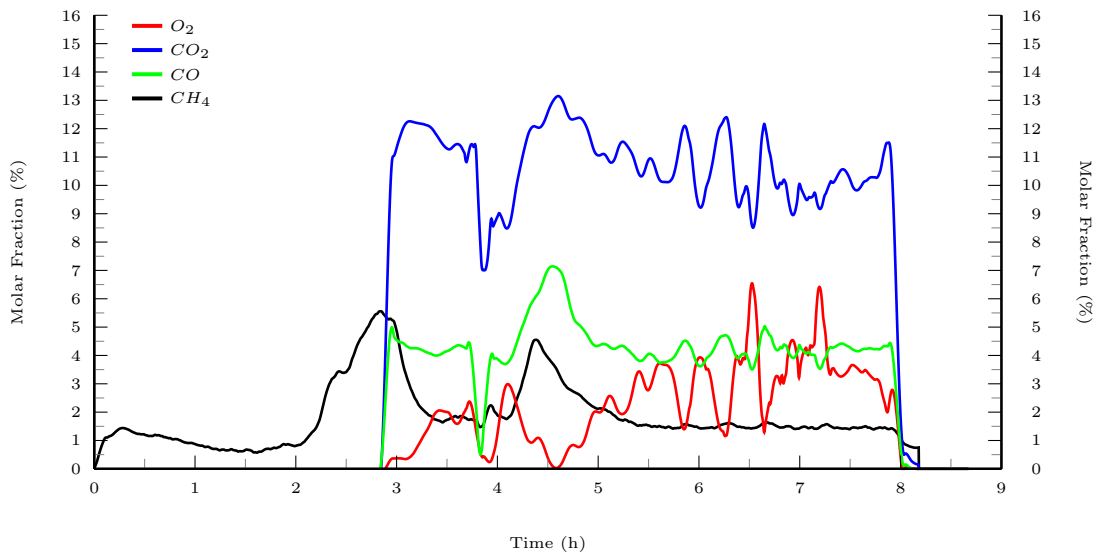

Figure 3.16: Gas data for RUN 5.

The interrupted run stabilized quickly. For the stabilized region a velocity of 14.4 cm/h was obtained.[7] Due to the leak, production data can only give a rough estimate (see Table A.10). Stoichiometry-wise oxygen reactions happened in a HTO regime (see Eq. 3.8). Compared with gas phase parameters from other runs, results for RUN 5 (see Table A.16) were in the same range. It should be pointed out, though, that m yielded the lowest value of all runs.

[6]This coarse sand/clay combination has no corresponding kinetic cell experiment. In terms of surface area, it is ranked between the sand/clay combination and coarse sand.

[7](with 95 % confidence bounds: [13.9 14.9] cm/h)

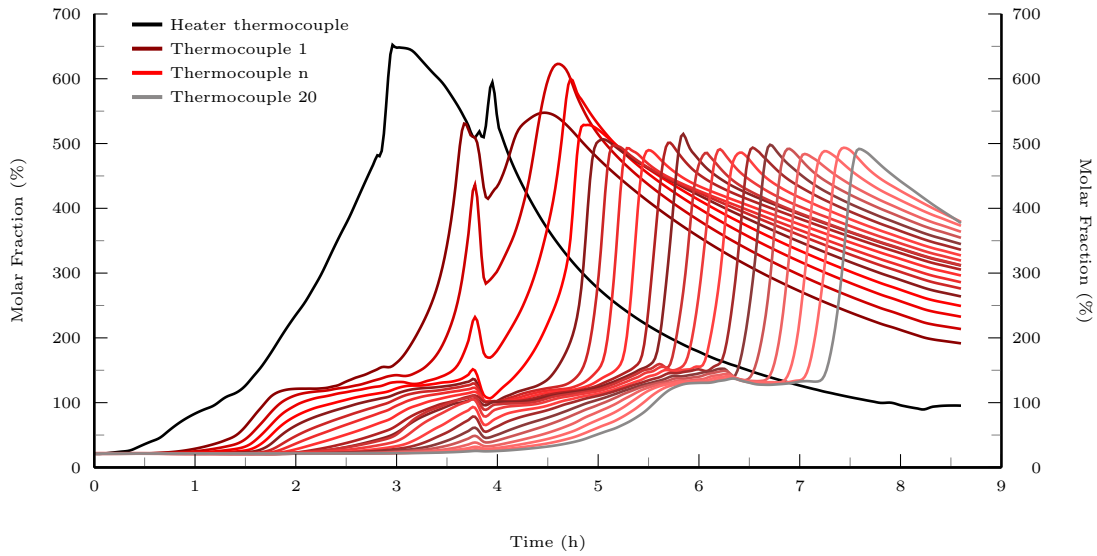

Figure 3.17: Temperature profile for RUN 5.

$$CH_{1.42} + 1.38O_2 + 5.28N_2 \rightarrow$$
$$0.71CO_2 + 0.29CO + 0.17O_2 + 0.71H_2O + 5.28N_2 \quad (3.8)$$

In terms of operational conditions (see Table A.15) RUN 5 consumed more fuel in total than any other run what may be a result of reduced surface area.

3.7.6 RUN 6.

As RUN 5, RUN 6 focuses on the effect of reduced surface area. Again a 16# sand instead of a 60 # sand was used. In addition no clay was used at all (see Table A.6). This combustion tube corresponds to the kinetic cell experiment using only the coarse sand (for activation energy see Fig. 2.8).

The altered composition caused a dramatic change in behaviour. During packing it was obvious that the matrix was not able to hold back the water. As a result water was produced by pure gravity drainage once the tube was brought into vertical position (see Table A.11 for production data). Though the ignition temperature looked promising (see Fig. 3.19) the combustion front could not be sustained and

died. The velocity of the dying front was calculated with 4.8 *cm/h*.[8]

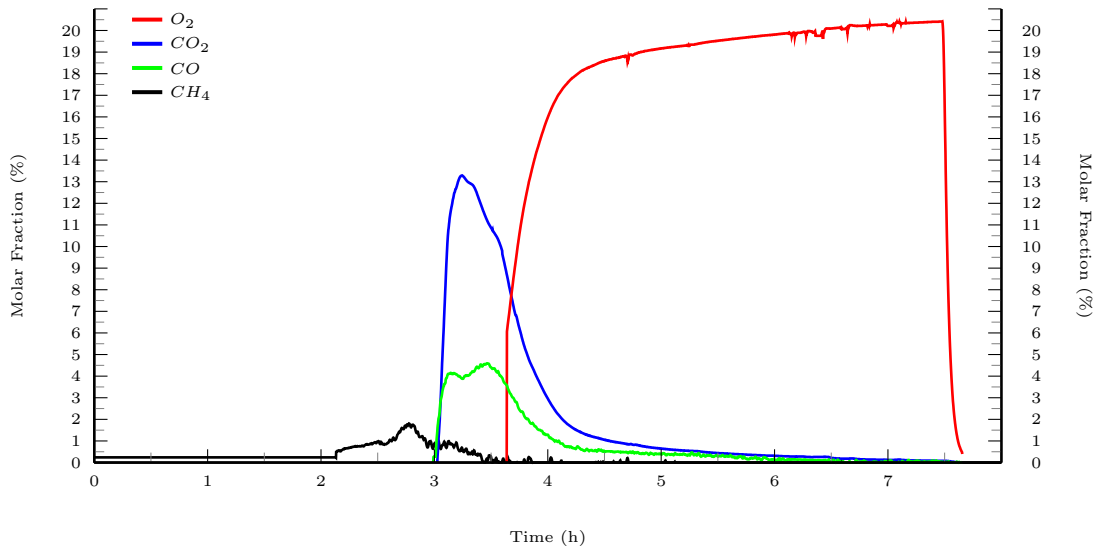

Figure 3.18: Gas data for RUN 6.

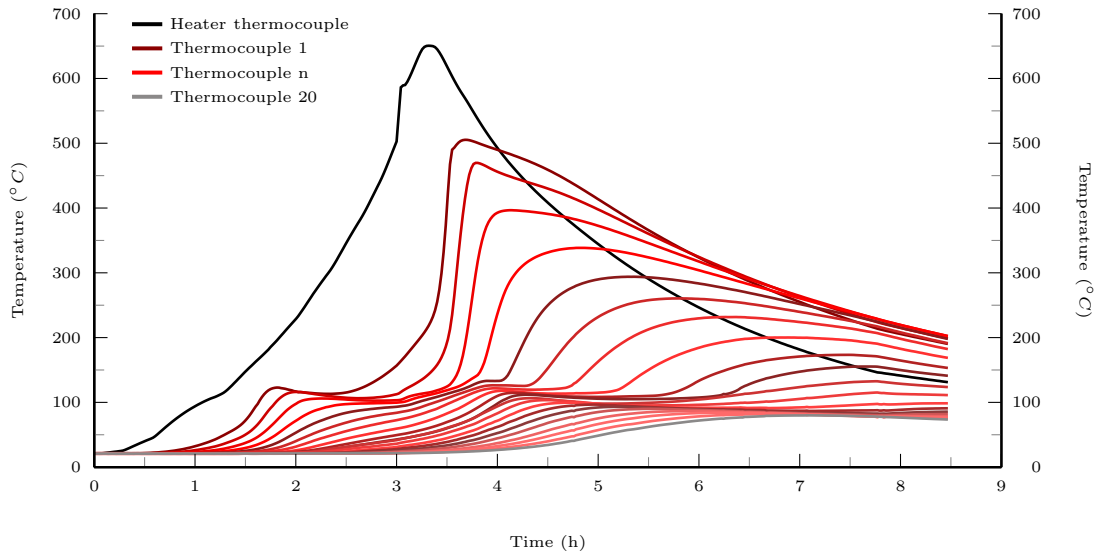

Figure 3.19: Temperature profile for RUN 6.

Determining the stoichiometry for this special case it comes as no surprise that we obtain the highest H/C ratio of all runs. However, Eq. 3.1 is only true as long as

[8](with 95% confidence bounds: [4.5 5.4] *cm/h*)

temperatures of the front is in the HTO region i.e. above 400°C. There are two main reasons this run failed. First, the matrix was not able to hold back the water. At time of ignition the top of the tube was at residual water saturation.[9] Hence the process was not able to take full advantage of the heat capacity of water etc. Second, effective activation energies derived from kinetic cell experiments using the same matrix composition indicated a significant energy barrier at the end of the LTO region (see Fig. 2.8). It was concluded, that the ability to create coke was greatly impaired by the barrier. This is partly reflected by the lowest amount of pyrolysis coke collected for all runs (see Table A.17).

$$\begin{aligned} &CH_{2.18} + 18.26O_2 + 69.97N_2 \rightarrow \\ &0.68CO_2 + 0.32CO + 16.88O_2 + 1.09H_2O + 69.97N_2 \end{aligned} \tag{3.9}$$

When comparing gas phase parameters (see Table A.16) as well as operational data (see Table A.15) with results from other runs you have to keep in mind that the run was not successful. For example total fuel consumed is the lowest for all runs and the oil was produced by air pushing it rather than the combustion process.[10]

3.7.7 RUN 7.

The main purpose of the RUN 7 was to determine the minimum air flux required in order to sustain the combustion front. At low air flow rates, it is more likely that the oxygen is completely consumed by the fuel and reacting volatile material. As opposed to previous runs, the combustion becomes oxygen-limited instead of reaction-limited. The sample mixture (see Table A.6 on page 66) is comparable to sample mixtures used in RUN 1 through RUN 4.

Instead of using a constant air flow rate of 3 l/min a variable flow rate program as shown in Fig. 3.20 was applied. Air injection commenced after 2 hours with 2 l/min. The flow rate was then gradually decreased to 1.5 l/min and held constant

[9] The initial oil saturation was the same as for the other combustion tube experiments.
[10] RUN 6 had the highest absolute permeability.

for about 2.5 hours. According to the temperature profile, the combustion front can be sustained with 1.5 l/min (see Fig. 3.21). Therefore, the flow rate was further decreased to 1 l/min. At this point the combustion front temperature started to decrease. However, the combustion front may still be able propagate at this flow rate because combustion front temperatures are above 400°C. A future experiment starting at a flow rate of 1.5 l/min and subsequent decrease should clarify this matter. The combustion front velocity for an airflow rate of 1.5 l/min was about 7.6 cm/h.[11]

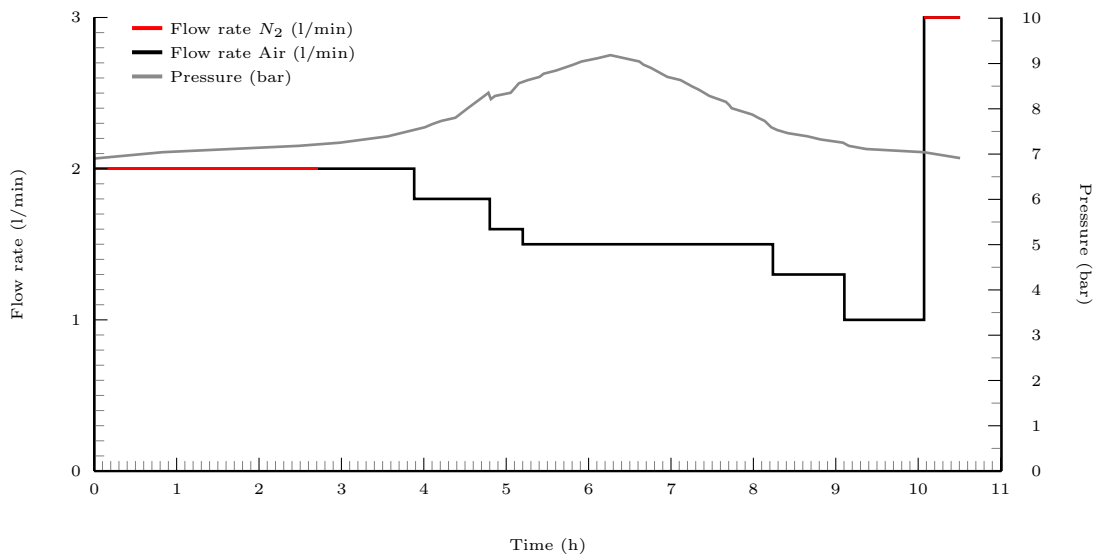

Figure 3.20: Flow rate for RUN 7.

In order to minimize sampling problems a new production vessel design was employed. The new design allowed production of all liquids without the need of sampling and therefore interrupting the air flow. Consequently, the gas production data was free of spikes (see Fig 3.22). In addition, the pressure was not held constant (see Fig. 3.20). During the experiment, the pressure increased from initially 6.89 bar (100 psi) to 9.2 bar (133 psi) going back to 6.89 bar again. It is assumed, that the pressure increase and subsequent drop correlate with oil production. Once the oil bank reaches the production part of the tube the oil is gradually discharged and pressure starts to drop accordingly.

[11] With 95 % confidence bounds: [7.1 8.1] cm/h.

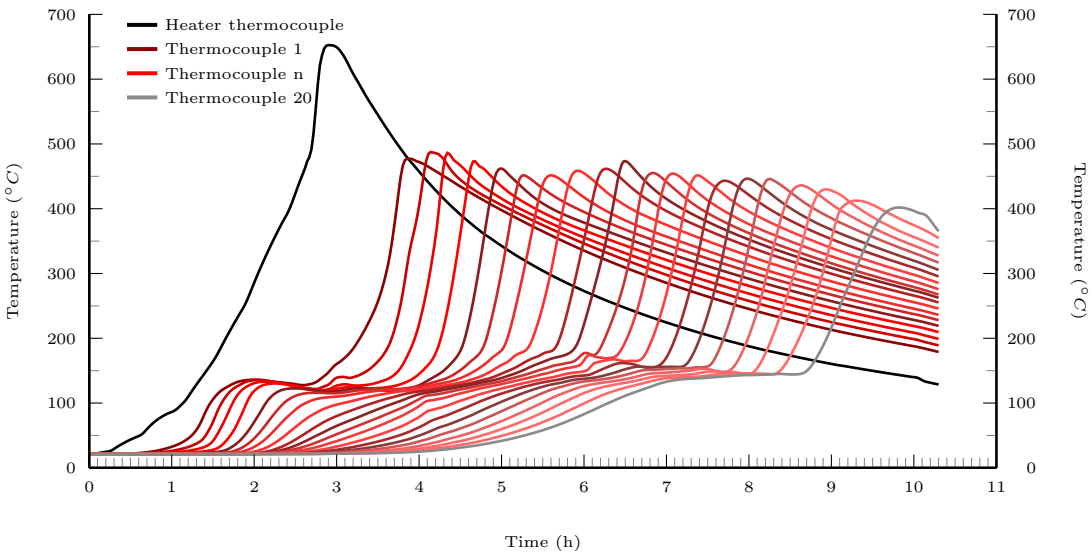

Figure 3.21: Temperature profile for RUN 7.

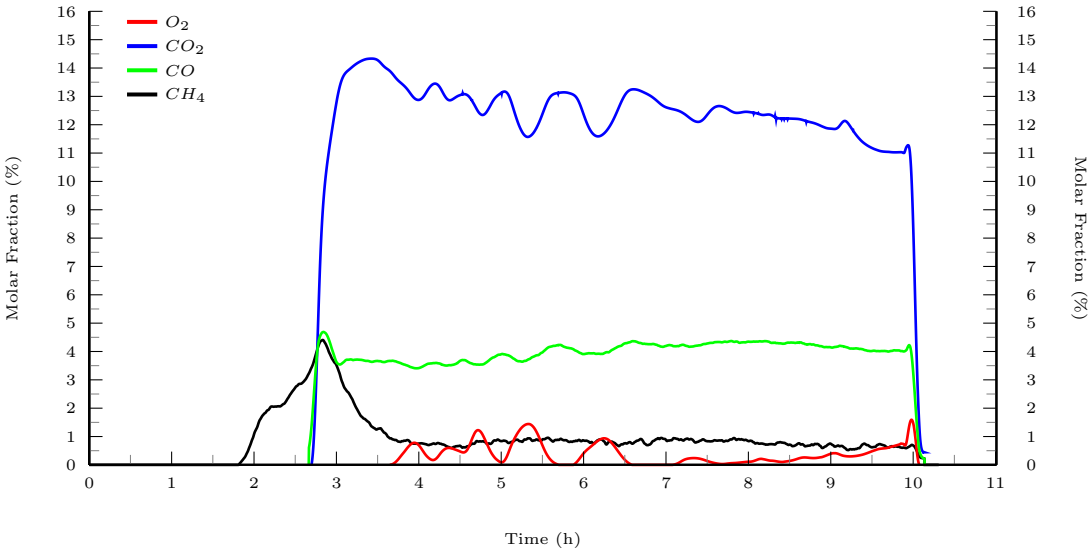

Figure 3.22: Gas data for RUN 7.

In terms of gas production data the amplitude of oscillations were reduced significantly (see Fig. 3.22). This supports the assumptions made on page 28 that packing is solely responsible for oscillations. Again, the frequency is too small that a geomechanical issue could be solely responsible. Though gas production data suggests a very efficient run - most of the oxygen is converted to CO_2 and CO respectively - oil recovery for the swept zone is only 54% (see table A.15). Fig. 3.22 shows that the entire oxygen injected is consumed to a great extent during the entire experiment. This might seem favorable in terms of efficiency but apparently there is a trade off i.e. lower recovery. Overall the questions is what would be the optimum air flow rate?

The driving mechanisms in a combustion tube run are two fold, though related to each other. On the one hand we have the combination of gravity drainage and air injected (flow rate) pushing the oil towards the lower end of the tube. This is especially true for the non-wetting fluid. On the other hand we have the the combustion process driving the liquid production by means of viscosity reduction, gas drive, miscible flooding etc. Determining to which extent a certain recovery mechanism contributed to oil recovery is challenging, especially for higher flow rates. For RUN 7 we can assume that the combustion process was the main driving force due to the very low flow rates of air injected. Again, in terms of oxygen burning efficiency this seems favourable because all air injected was consumed. Translating this to the field case, we would have made optimum use of the compressor because we did not waste injection capacity. Apparently, this came at the price of lower recovery. When the flow rate is too low, there is not enough oxygen available to burn enough coke for an efficient displacement. Looking at Fig. B.14 we can see that that even the less consolidated zone[12] is comparably dark indicating that coke was only partially burned. Excessively high flow rates are no good either. Especially for the field case, oxygen breakthrough at the producer posses a considerable threat. Importantly, from an economic point of view, compressor capacity must not be wasted. Again, determining the optimum air flux is challenging. Making matters worse is the fact that we do not need to burn all the coke created to achieve optimum economics. Using combustion tube runs to determine optimum air flow rate is not practical. It would

[12]The less consolidated zone has lower oil saturation compared to consolidates zone.

require an extensive number of runs. Besides, we must not forget for the setup used higher airflow rates are required to compensate for heat losses. Hence, even minimum flow rates have to be interpreted with great care. Compared with RUN 3 (see page 34) and RUN 4 (see page 34) the higher H/C ratio of 1.45 (see Table A.16 and Eq. 3.10) indicates that it was comparably hard to maintain a HTO regime. This points out the importance of a high enough air flux so enough coke is burned to maintain a high enough temperature.

$$\begin{aligned} &CH_{1.45} + 1.26O_2 + 4.84N_2 \;\rightarrow \\ &0.75CO_2 + 0.25CO + 0.02O_2 + 0.72H_2O + 4.84N_2 \end{aligned} \tag{3.10}$$

Looking at Fig 3.23 we can see that with decreasing air flow rate the H/C ratio tends to increase. Once the flow rate is $1l/min$ the H/C drops above 1.7. This is an indication that $1l/min$ is a critical value to sustain the combustion front for this experimental setup. We can also see that with decreasing flow rate less and less oxygen is needed to burn the coke because coke deposition itself decreases with dropping temperature.

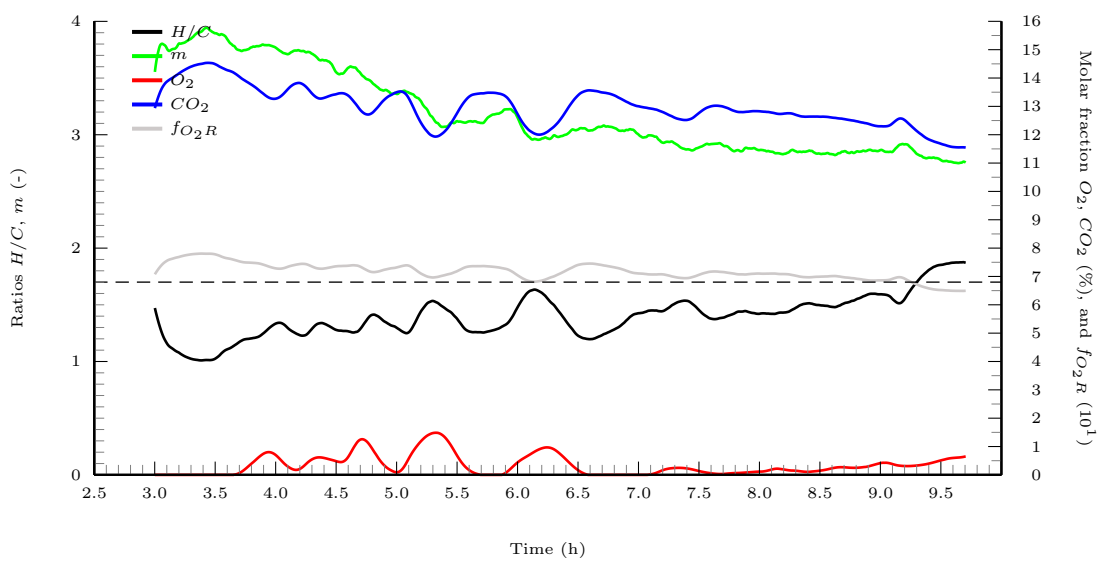

Figure 3.23: Selected parameters for entire RUN 7.

Chapter 4

Upscaling for In-Situ Combustion

Currently, most simulation studies related to in-situ combustion (ISC) are restricted to modelling small laboratory scale problems such as kinetic cell and combustion tube experiments. The transition from laboratory to field scale is still an unsolved problem due to the very nature of the ISC process in combination with the discretization techniques used to solve the convection-diffusion equations. In its simplest form we use the following centered differencing scheme for approximation of a first derivative transport term:

$$\frac{T_{i+1} - T_{i-1}}{2\Delta x} = \frac{\partial T}{\partial x}(x_i) + \frac{(\Delta x)^2}{6}\frac{\partial^3 T}{\partial x^3}(\xi), \quad x_{i-1} \leq \xi \leq x_{i+1} \tag{4.1}$$

If T is sufficiently smooth, the scheme has $\mathcal{O}((\Delta x)^2)$ accuracy. The scheme, however, is well known to yield stability problems [31, 55]. Instead of the central difference quotient a one-sided difference approximation in the direction of flow is preferably used to foster stability. The scheme is given by

$$\frac{T_i - T_{i-1}}{\Delta x} = \frac{\partial T}{\partial x}(x_i) - \frac{\Delta x}{2}\frac{\partial^2 T}{\partial x^2}(\xi), \quad x_{i-1} \leq \xi \leq x_i \tag{4.2}$$

The accuracy for Eqn. 4.2 is only $\mathcal{O}(\Delta x)$ and we can show using a Taylor series that

$$\begin{aligned}\frac{T_i - T_{i-1}}{\Delta x} &= \frac{T_{i+1} - T_{i-1}}{2\Delta x} - \frac{\Delta x}{2}\left(\frac{T_{i+1} - 2T_i + T_{i-1}}{(\Delta x)^2}\right) \\ &= \frac{\partial T}{\partial x}(x_i) - \frac{\Delta x}{2}\frac{\partial^2 T}{\partial x^2}(x_i) + \mathcal{O}((\Delta x)^2) \qquad (4.3)\end{aligned}$$

Eqn. 4.3 is also referred to as upwind differencing and is essentially a $\mathcal{O}((\Delta x)^2)$ approximation to

$$\frac{\partial T}{\partial x}(x_i) - \frac{\Delta x}{2}\frac{\partial^2 T}{\partial x^2}(x_i) \qquad (4.4)$$

instead of $\partial T/\partial x\ (x_i)$. With $\partial^2 T/\partial x^2$ being a physical diffusion-like term this introduced an *artificial dispersion* of size $\Delta x/2$ [19]. Though artificial dispersion does help to stabilize the difference method, the error induced in reservoir simulation is problematic. The magnitude of dispersion is directly proportional to the mesh spacing Δx and is likely to smooth out sharp fronts. Fig. 4.1 illustrates what happens in the case of loss of physics due to excessive smoothing and/or dispersion. Opposed to the true temperature distribution in reservoir, cell block averaging and dispersion reduce the maximum temperature below the reaction level prohibiting reactions from taking place.

For ISC the chemical reaction front is physically very narrow and requires centimeter-sized grids to be captured accurately. This is orders of magnitude smaller than affordable grid block sizes for full field reservoir models. Accordingly, severe grid size effects are encountered in full field-scale simulation making performance predictions infeasible [17, 28]. In order to mitigate grid size effects both empirical [36] and specialized numerical techniques [26, 33], have been proposed with mixed results. None of the techniques, however, made field-scale simulation practical in a commercial environment.

In 2011, Zhu et al. proposed a method based on a non-Arrhenius kinetic upscaling approach similar to the classical analytical model of Gates and Ramey [25]. Instead of resolving the combustion front on the grid, a subgrid-scale model is utilized capturing

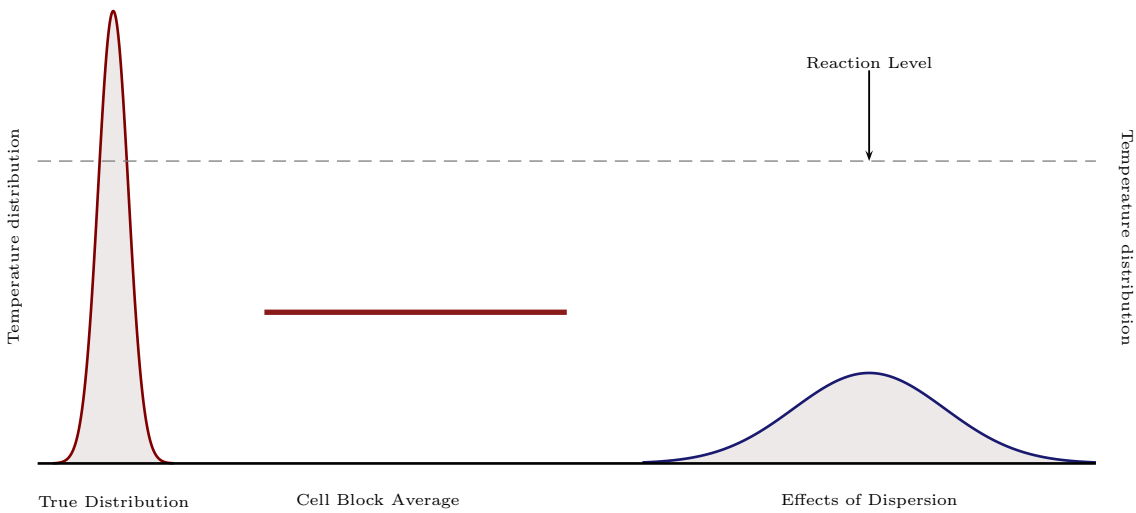

Figure 4.1: Front resolution in thermal simulation (after [19]).

the overall effects of the combustion reactions on flow and transport. In essence the approach assumes constant pre-determined lay-down of fuel at the beginning of the simulation. The reaction model is described using two pseudo reactions. At the beginning of the simulation the oil (Oil_1) is split up into an inert component (Oil_2) and coke.

$$1\ Oil_1^l \longrightarrow\ (1-x)\ Oil_2^l\ (\text{inert})\ +\ x\ Coke^s \tag{4.5}$$

The coke is then burned in the presence of oxygen according to the subsequent reaction:

$$Coke^s\ +\ O_2^g + N_2^g\ \longrightarrow CO^g\ +\ CO_2^g + H_2O\ +\ N_2^g \tag{4.6}$$

The pre-determined amount of coke to be oxidized (referred to as "x") can be determined as outlined in [3].

The governing equations for mass and energy transport in reactive thermal compositional simulations are

$$\frac{\partial C_i}{\partial t} + \boldsymbol{\nabla} q_i = Q_i^{well} + Q_i^{reac} \tag{4.7}$$

$$\frac{\partial U_t}{\partial t} + \boldsymbol{\nabla}\left(q^{h,adv} + q^{h,cond}\right) = Q^{h,well} + Q^{h,reac} \tag{4.8}$$

where C_i is the mass composition of i-th component, U_t is the total internal energy, q_i and $q^{h,adv}$ are advective mass and energy fluxes, Q_i^{well} and $Q^{h,well}$ are the well terms, and Q_i^{reac} and $Q^{h,reac}$ are the reaction terms.

Traditionally, Arrhenius kinetics are used for modelling ISC reactions. The reaction rate for a grid cell is then given by

$$Q_i^{reac} = V_b \times A \times e^{\left(\frac{-E_a}{R \times T}\right)} \times \prod_j (C_j)^n \tag{4.9}$$

where V_b is the rock bulk volume, A is the Arrhenius constant or pre-exponential factor, E_a is the activation energy, R is the ideal gas constant, T is the local absolute temperature, n is the reaction order, and C_j is the j-th reactant concentration. C_j is defined as

$$C_j = \Phi \times b_p \times S_p \times x_j \tag{4.10}$$

where p depicts the phase (oil, gas, or water), Φ is the porosity, S is the saturation, b is the molar density, and x is the mole fraction.

The approach presented in [57] assumes an activation energy E_a of zero, reducing Q_i^{reac} essentially to

$$Q_i^{reac} = V_b \times A \times \prod_j (C_j)^n \tag{4.11}$$

Consequently, the burning reaction taking place during simulation is independent of temperature. In the presence of oxygen, coke will burn unconditionally. It has to be noted that this approach can only be considered in case of successful laboratory combustion tube runs.

4.1 Challenges

4.1.1 Premature Gas Breakthrough

Before the method was implemented in a commercial simulator, a series of tests were carried out to investigate simulator behavior and limitations. Previous investigations reported instantaneous gas breakthrough at the producer. As soon as gas was injected, it appeared at the producer. A basic producer/injector model as shown in Fig. 4.2 was set up to investigate this behavior. The well placement and grid dimensions were in accordance with the sector model to be history matched. The $dx \times dy \times dz$ dimensions of a cell were set to $32ft \times 32ft \times 2ft$ ($9.75m \times 9.75m \times 0.61$).[1] The distance between injector and producer is, therefore, given with $288ft$ or $88m$ respectively.

The premature breakthrough behavior could be reproduced. As soon as nitrogen was injected, the gas appeared at the producer (see Fig. 4.5). The same behavior was encountered for oxygen injection. Given that the reaction model proposed in [57] assumes zero activation energy (see Eqn. 4.11) the premature air breakthrough is especially troublesome. As soon as oxygen is injected we can observe a *burning producer* (see Fig. 4.3). That is, the temperature at the producer starts to rise as a result of coke being oxidized. The situation gets worse because air injected travels in the uppermost layer, burning fuel unconditionally. Thereby a high permeability flow path is created through which air channels preferably making it impossible to establish a combustion front. The result is depicted in Fig. 4.4. The combustion front basically jumps from the injector to the producer.

There are two main reasons why this is happening. First, due to the discrete nature of the simulation, numerical dispersion is introduced giving rise to a combustion front

[1] This gives a total bulk volume of $352ft \times 352ft \times 22ft = 1,362,944ft^3$ or $38,594m^3$.

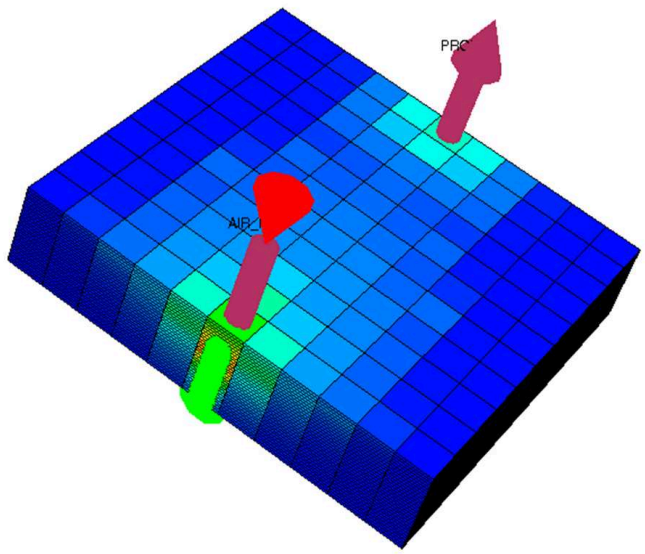

Figure 4.2: Injector/Producer configuration. Grid block dimensions are $32ft \times 32ft \times 2ft$ with 33 blocks vertically and 11×11 blocks laterally.

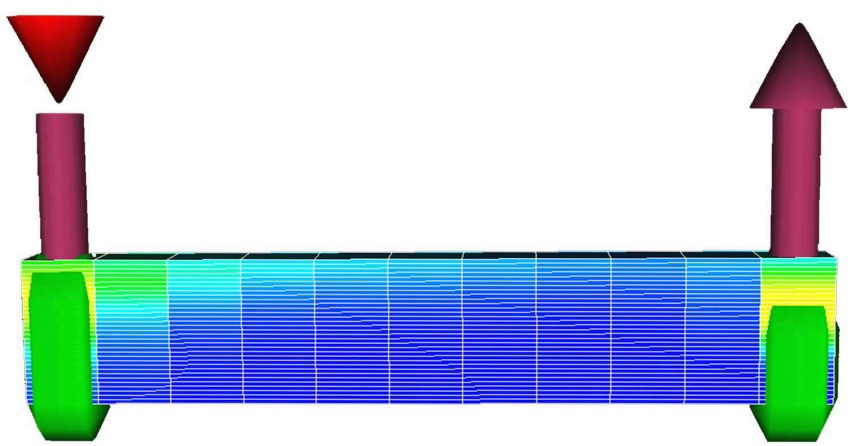

Figure 4.3: Temperature distribution of a cross section of Fig. 4.2 showing *burning producer* behavior. Air is injected on the right. Though the combustion front is only partially established, the temperature at the producer is already at $750°F$ (yellow color) suggesting the combustion front has already arrived.

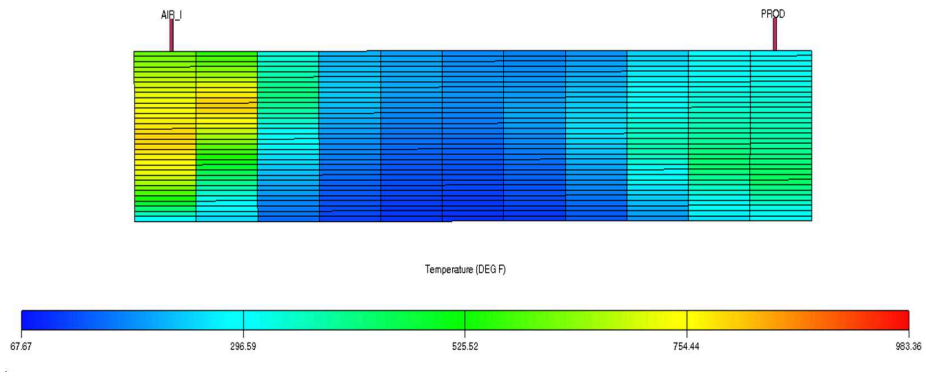

Figure 4.4: Air injected (left side) travels in the uppermost layer due to gravity segregation. A high permeability flow path is created through which air channels preferably making it impossible to establish a combustion front. The combustion front jumps from the injector to the producer.

travelling along with the dispersion (combination of Eqn. 4.4 and Eqn. 4.11). If gas enters a grid block at one end, it immediately appears at the other end of the block.

Second, the mobility ratio is highly unfavorable and large differences in density result in a severe gravity override. While numerical dispersion is an artifact originating from the discretizing scheme used, gravity override is not. Gravity override is also observed in the field. Given the poor injectivity at the beginning of injection, it is common practice to establish air permeability first by injecting air several hours before ignition. Apparently, this can not be done in the simulation case. At the beginning of the simulation coke is already in place and burns in the presence of air unconditionally. The reason this behaviour was not reported by Zhu et al. previously is due to different initial conditions used. In their simulation cases, the initial saturations are comparable to combustion tube experiments. An inert gas phase was already in place mitigating any injectivity problems by establishing gas permeability a priori. The simulation model employed in this investigation, however, used initial saturations observed for the field (oil and water only). For history matching purposes and the sake of consistency, no inert gas can be assumed at the beginning of the simulation.

As mentioned above instantaneous gas breakthrough of gas was reported for non-related cases. For those cases, it was suggested to modify relative permeability curves.

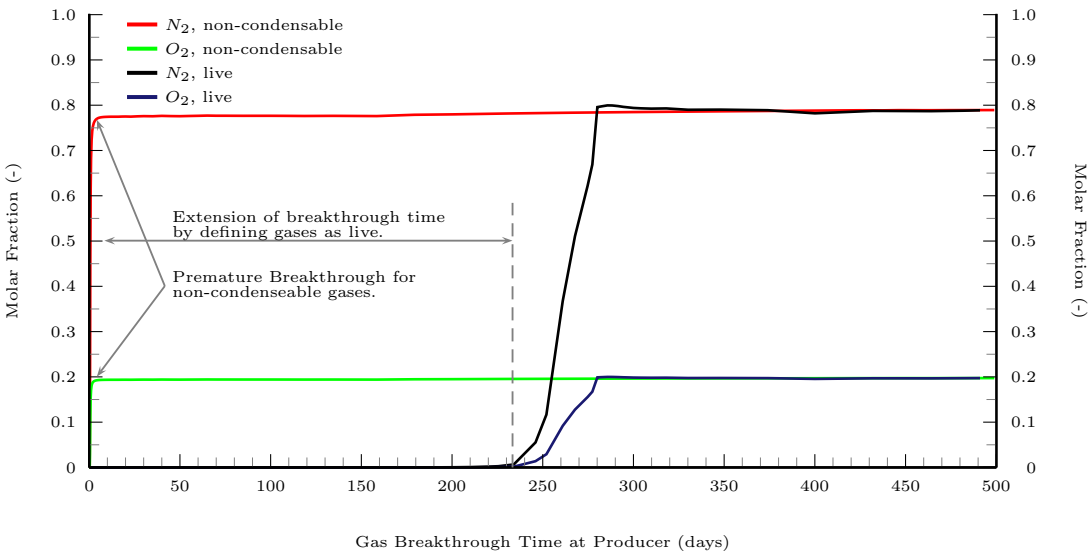

Figure 4.5: Example of premature gas breakthrough. If air injected is treated as non-condenseable, instantaneous breakthrough is observed at the producer. This is especially troublesome in combination with the *x-method*. That is, air and combustion front travel at the same speed. Consequently, the front arrives at the producer too early. If the gas is treated as *live*, premature breakthrough is prevented.

This approach, however, did not yield any useful results.

Another possibility to prevent instantaneous gas breakthrough at the producer is to treat gases as *live* components instead of *non-condenseable*. Fig. 4.5 summarizes breakthrough times for the immiscible and miscible case. In the case of instantaneous breakthrough both oxygen and nitrogen were treated as immiscible. If gases are treated as live components the effect is apparent. Air requires now around 200 days to travel from the producer to the injector. Arguably, this is in contrast to PVT experiments generally suggesting that for heavy oils mixing can be neglected.

Treating gases as miscible suggests to be computationally more expensive. Investigations on calculation time required for different sets of gases being set to *live*, however, were inconclusive.

Reactions and Consistency

In commercial applications, simulation time is critical. Any reaction or component added, introduces an additional complication resulting in increased simulation time. Consequently, the number of components and reactions should be held to a minimum. The original approach presented in [57] suggests two pseudo reactions. These reactions can be reduced to one reaction which essentially represents the *high temperature oxidation* (HTO) reaction as shown in [27]. The HTO reaction can be further simplified by combining carbon dioxide (CO_2) and carbon monoxide (CO) or neglecting CO completely.

Depending on the production history, the HTO reaction may require an additional modification. Usually, before a field is developed by means of combustion other thermal recovery techniques like steam injection etc. are employed. The original approach treats fuel - physically correct - as a solid. Consequently, this leads to inconsistencies because even before combustion is initiated, fuel in form of a solid phase is present in the reservoir. One possibility to avoid this contradiction is to substitute fuel with the original oil in place. The caveat is, that this oil turned fuel must not be subject to viscosity reduction due to a temperature increase. In this case, no relative permeability adjustments are required. The only reaction required is then given by

$$x\ Fuel^{l/s} + \alpha O_2^g + \beta N_2^g \longrightarrow \gamma CO_y^g + \eta H_2O + \beta N_2^g + Heat \quad (4.12)$$

$$\begin{aligned} x &\ \ldots\ \text{predetermined amount of fuel} \\ CO_y^g &\ \ldots\ CO_2 \text{ and } CO \text{ combined} \\ \alpha, \beta, \gamma, \eta &\ \ldots\ \text{stoichiometric coefficients} \end{aligned}$$

Whether or not the coke is treated as solid or liquid in the simulation model is subject to discussion.

The reduced reaction model (Eqn. 4.12) was compared against the following kinetic reaction model ([18]),

$$
\begin{aligned}
Oil + O_2 &\longrightarrow Coke_1 \\
Coke_1 + O_2 &\longrightarrow Coke_2 + CO + CO_2 + H_2O \\
Coke_2 + O_2 &\longrightarrow CO + CO_2 + H_2O
\end{aligned}
$$

and the upscaled reaction model as proposed by Zhu et al. (see Eqn. 4.5 and Eqn. 4.6) using a 1-D combustion tube simulation (see Fig. 4.6). The kinetic model has a resolution of 0.14 inches (0.36 cm) with a total of 602 cells giving a total length of 7.11 ft (2.16 m) for the combustion tube.

For the upscaled case, the number of cells in Fig. 4.6 is reduced to 60 resulting in a cell width of 1.42 inches (3.6 cm). Results for total oil production and production rate are shown in Fig. 4.7 and Fig. 4.8, respectively. All models yield the same total oil production. The reduced reaction model (Eqn. 4.12), however, follows the production history of the full kinetic model more closely.

Fig. 4.9 summarizes the simulation time for three different cases. The method of Zhu et al. slashes simulation time from 600 seconds to 20 seconds yielding a decrease in simulation time by a factor of thirty. Using the modified approach presented in this report, the simulation time is further decreased to 10 seconds which is a 50% performance increase over the original method. It has to be pointed out that reduction in simulation time for 1D cases does not scale linearly for 3D cases.

4.1.2 Upscaling of Reaction Kinetics

Upscaling of reaction kinetics is arguably the most challenging part when it comes to ISC field scale simulation. As illustrated in Fig. 4.1, mesh spacing has a strong impact whether or not an ISC front can be sustained in a simulation for given reaction

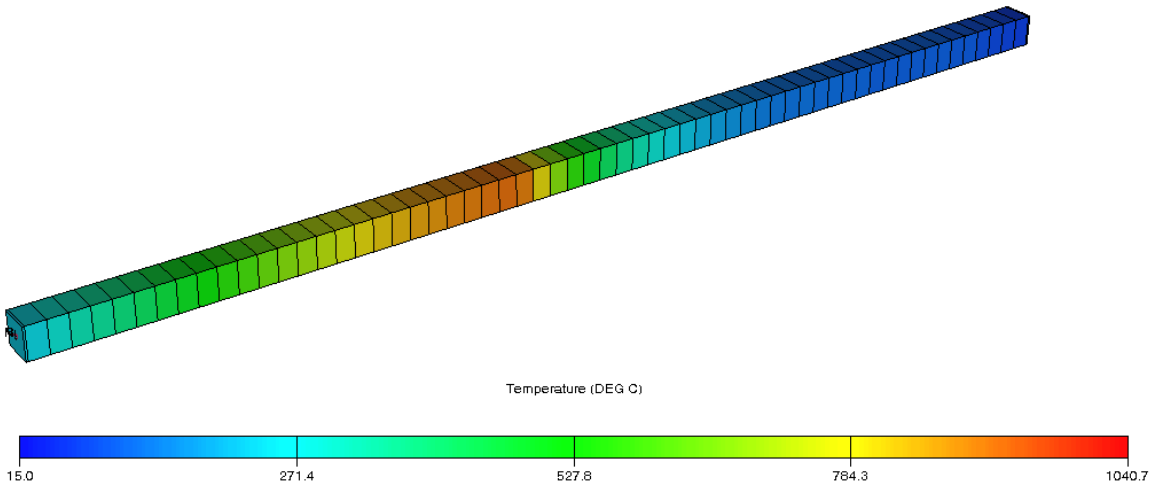

Figure 4.6: Combustion tube configuration for comparison of kinetic and upscaled models.

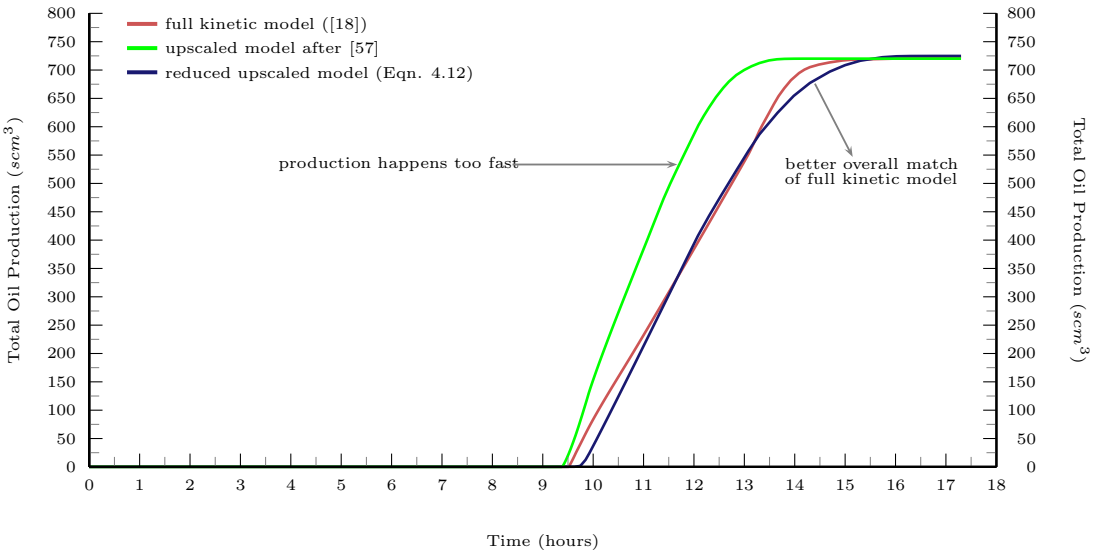

Figure 4.7: Comparison of total oil produced for full kinetic and upscaled models.

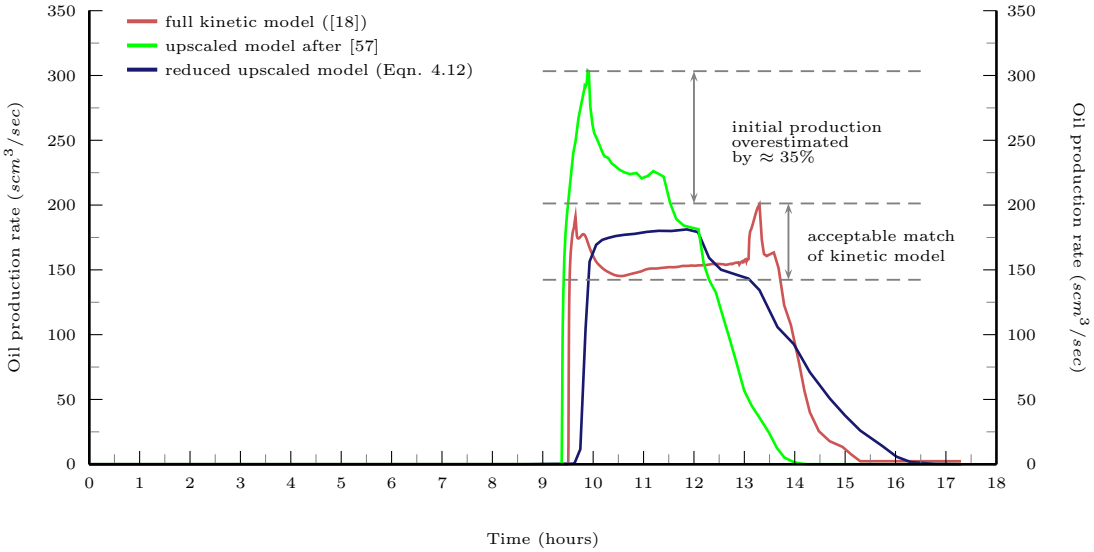

Figure 4.8: Comparison of oil production rate for full kinetic model and upscaled models.

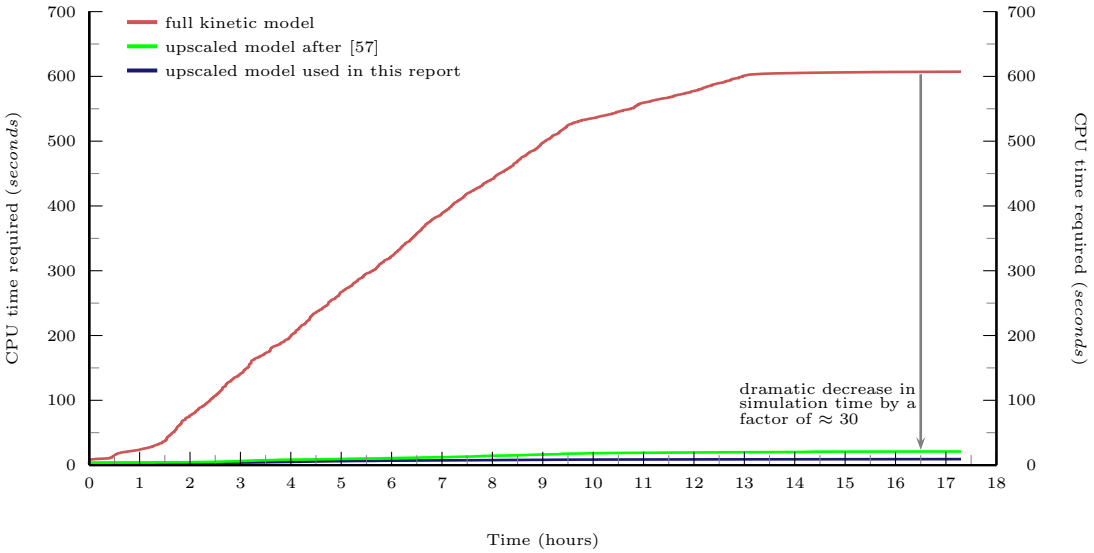

Figure 4.9: Comparison of CPU time required for simulation for full kinetic and upscaled models.

set. Even more a grid will likely have a higher vertical than lateral resolution to honor any geological information provided. In addition severe grid orientation effects can occur. This is especially true in case of high mobility ratios. Special operators (e.g. nine-point stencil for multi-point flux approximation) currently implemented in commercial simulation software are of no use for this field scale simulation because of computational complexity and inability to be used in parallel mode.

A first step to get rid of grid size dependency for reaction kinetics is setting the activation energy to zero as done in [57]. Consequently, there is no reaction level as shown in Fig. 4.1 anymore. Then, the rate of a chemical reaction depends on porosity, component concentrations, phases, and reaction rate constant only. In essence, fuel is burned in the presence of oxygen unconditionally. It has to be emphasized, again, that this can only be done for an oil for which laboratory combustion tube runs were successful.

The correct treatment of reaction rate constant and enthalpy of reaction is more complicated due to grid size dependency. No rigorous approach exists yet. Regarding the reaction rate constants, Zhu et al. suggest a very large constants for the pseudo reactions. Essentially they are treated as equilibrium reactions. Unfortunately, the application of large reaction rate constants can result in severe numerical difficulties (convergence issues) especially for field scale simulation.

A different approach could be as follows. In case historical production data is available a lot can be learned about the movement of the combustion front. In general a production well needs to be shut in when the combustion front arrives. Subsequently, the well is usually turned into an injector. Production data and shut-in time of a well not only help to estimate the velocity of the front but also the vertical sweep efficiency. A mock-up model as shown in Fig. 4.2 can then be used to calibrate reaction rates. It was found that lower reaction rate constants mitigate numerical difficulties and help to establish a more physical behavior of the combustion front for this case.

4.1.3 Viscosity and Temperature

The main idea behind combustion is to reduce the viscosity of a heavy oil by generating heat in-situ. Accordingly, the viscosity of the oil is a mainly a function of temperature that is governed by the heat released (enthalpy) of the burning reaction. Combustion tube experiments give reasonable estimates of the front temperature. The problem is how to define front temperature in the simulation?

From a conventional upscaling point of view, the temperature of a cell block will be some average value (see Fig. 4.1). This average value will likely be, depending on the grid size, below the the front temperature observed. As a result, the temperature will be below the reaction level. Regarding the reaction this is no problem because the kinetics used are temperature independent (see Eqn. 4.11). Regarding the viscosity reduction of oil, however, this is a major issue. Though reactions are happening we are not able to mobilize the oil sufficiently and production will stay behind expectations. If we increase the enthalpy of the reaction to obtain grid block temperatures comparable to front temperatures observed in the lab (which is clearly a contradiction) we possibly mobilize too much oil too early.

For a given enthalpy value there is a dominating maximum temperature.[2] If this maximum temperature is below combustion tube front temperatures we need to tell the simulator, that this temperature actually corresponds to the maximum viscosity reduction. Vice versa, in case the maximum temperature is above combustion tube front temperature we need to set a limit in viscosity reduction.

4.2 Results and Conclusions

The method presented in [57] in combination with the modifications presented in this report provide a viable basis for field scale ISC simulation when applied responsibly. The approach was successfully used for history matching 30 years of hot production of one of largest ISC projects in the world. It was found that a successful match

[2]Here *dominating* refers to the fact that some cells sometimes show significantly higher temperatures than others. E.g. in Fig. 4.10 a couple of cells reach temperatures above $2000°F$ ($1100°C$). Usually these cells can be found near the injector.

depends on the proper combination of gas breakthrough time, reaction rate, and viscosity. With substantial effort, gas breakthrough time and reaction rate can be tuned in a way that no viscosity adjustments are required. Fig. 4.10 and Fig. 4.11 show the improvements that can be made applying the techniques discussed in this report. Compared to Fig. 4.3 and Fig. 4.4 respectively, the combustion front shows more physical behaviour.

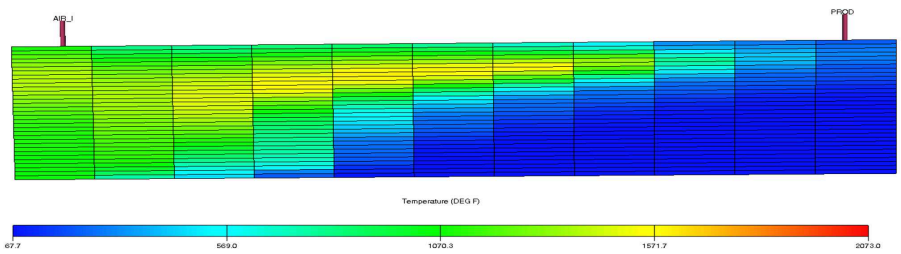

Figure 4.10: Temperature distribution after proper combination of reaction rate and gas miscibility. Compared to Fig. 4.4 a more realistic reaction combustion front is established.

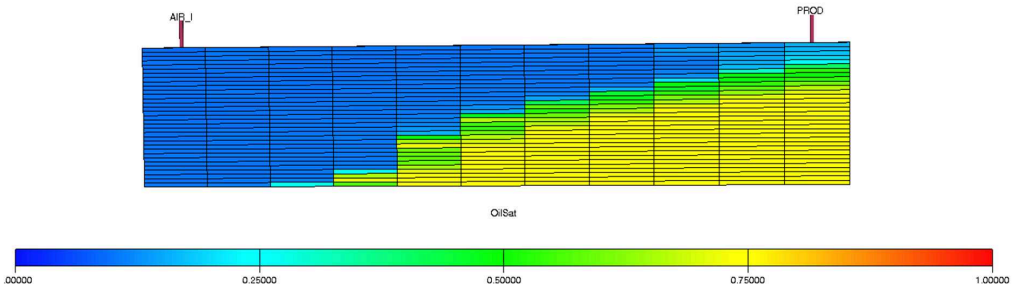

Figure 4.11: Distribution of oil saturation for temperature distribution in Fig. 4.10.

Again, it has to be pointed out that for the field case certain recognizable features seen in combustion tube simulation (e.g. sharp front) do not exist anymore. Furthermore, it was found that for certain settings, simulation results depend on CPU architecture used.

Chapter 5

Discussion and Conclusion

This master thesis summarizes the experimental efforts undertaken to describe the characteristics of a Central European crude oil with respect to the process of ISC. Combining RTO experiments with the isoconversional principle, apparent activation energy values were determined for several surface area cases. Iscoconversional results clearly show the impact of reduced surface area. Overall, reduction in surface area results in an increase of apparent activation energy for both LTO and HTO reactions. Using plots of activation energy versus temperature aids the derivation of customized reaction schemes ([15]) and allows the introduction of special characteristics that general purpose reaction schemes might not be able to cover. For the crude oil under investigation, a reaction scheme is currently in preparation. A major issue is how to model the local maximum right before the Death Valley (e.g. see Fig. 2.8) that apparently is an important characteristic of the crude oil. Narrow confidence bands for apparent activation energy illustrate little random error. Overall, the crude oil/rock combination shows good kinetics and a high tolerance regarding reduced surface area.

Combustion tube temperature profiles exhibit heating rates in the range of 10°C/min to 25°C/min, depending on the oil used. Also, before the combustion front arrives at a certain differential volume in the tube, this volume was already brought to steam temperature allowing volatile elements in the oil to evaporate. The questions are will behavior have an impact on governing reactions and do the apparent activation energies depend on heating rates. It is necessary, therefore, to apply a heating

scheme that resembles the combustion tube temperature profiles more accurately if these questions are to be answered. In short, the sample in the kinetic cell should first be heated up to steam temperature. The temperature is then held constant for a certain amount of time to mimic the temperature history in the combustion tube. Finally, a heating rate in accordance with combustion tube heating rates is applied. The isoconversional principle can be applied as usual because a linear heating history is not needed. For the field it is believed that heating rates are more in the range of 2°C/min ([22]). Hence, except for the preheating of the oil, heating rates do not need to be changed.

Another question is if a different span of heating rates should be used e.g. instead of heating rates from 1°C/min to 2°C/min with 0.2°C/min increments we could use a range of 1°C/min to 20°C/min with 4°C/min increments. It is still under debate to which extent the isoconversional principle requires heating rates close to each other. The isoconversional method is a comparably young method for analysis of ISC and we still need to unlock its full potential. For example isoconversion based on carbon dioxide production.

The effect of surface area was also noticeable for combustion tube runs. The tube run having the smallest surface area died. For the second run with reduced surface area an increased fuel consumption was calculated. At the same time, however, this run yielded the greatest recovery. The reason is, that in the tube several driving mechanisms need to be taken into account. The decrease in surface area - that is especially true when removing the clay - went hand in hand with an increase in permeability. Hence, gravity drainage and gases flushing the tube added substantially to the production. Recovery values from tube runs cannot be directly related to the field case. We must take into account both the different driving mechanisms and also the permeability of the sand pack is likely to be greater compared to the field. Permeability for the sand pack was determined to be in the range of 10 mD. Also, the H/C Ratio was the largest for the successful runs, indicating problems sustaining the front in the HTO region.

A significant air flow rate is crucial in order to sustain the combustion tube front. In Fig. 3.23, we saw that with decreasing air flow rate, the burning process shifts

from an HTO dominated regime (low H/C-ratio) into an LTO dominated regime (high H/C-ratio). For the field case, air flow rates are of great importance because they dictate economics to a great extent. If flow rates are too large, a lot of air and, therefore, compressor capacity is wasted. In addition, air breakthrough at the producer poses a safety hazard. Also, in order to sustain the combustion front, not all of the coke created needs to be burned. Low flow rates cause a shift from the HTO regime to the LTO regime to a point where the front cannot be sustained.

Regarding flue gas oscillations, we see a direct impact of air flow rate. Oscillations disappeared with decreasing air flow rate. Tracking the H/C-ratio over time the fuel laid down in the presence of air differs from from the fuel created in an oxygen deficient environment.

Specific conclusions from this study follow.

- Kinetic measurements interpreted using the isoconversional approach appear to be predictive of combustion tube success and are able to quantify the shift in kinetics as the surface area changes.

- Effluent gas composition oscillation measured during combustion tube experiments are shown to originate from both flow rate and packing heterogeneities.

- The H/C ratio reported for successful combustion tube runs ranges from 1.25 to 1.86 suggesting an HTO dominated regime, as do the peak temperatures measured.

- Air requirements for larger surface area experiments are calculated to be around 250 $m^3(ST)/m^3$. With decreased surface area an increase of air requirements up to 337 $m^3(ST)/m^3$ was observed.

Appendix A

Additional Tables

Table A.1: Reservoir Properties.

Property	Value
area	1.52 km^2
depth	$35 - 220$ m
dip	$5° - 8°$
net pay thickness	4-24 m
total pay	17 m
$p_{res,initial}$	$4 - 22$ bar
$T_{res,initial}$	$18°C$
ϕ	0.32
rock density	2643 kg/m^3

Table A.2: Bulk Mineralogy

Bulk Mineralogy	%
Quartz	67
Plagioclase	10
K-Feldspar	2
Calcite	1
Dolomite	< 0.5

Table A.3: Clay mineralogy by weight

Clay Mineralogy	%
Kaolinite	2
Chlorite	1
Illite	12
Mixed-layer illite-smectite (MXL I/S)	5
% Smectite in MXL I/S	60-70

Table A.4: Parameters calculated from sieve analysis.

D_{10}	0.08 mm
D_{30}	0.11 mm
D_{60}	0.17 mm
C_u	2.1
C_c	1.5

Table A.5: Summary of solid/liquid mixtures.

Recipe	Mesh size (#)	Sand (g)	Powdered Kaolinite (g)	Water (g)	Oil (g)
Production sand	see Fig. 2.4	50.00	2.00	4.00	2.00
Burned fine sand and clay	60#	50.00	2.00	4.00	2.00
Coarse sand only	16#	50.00	-	4.00	2.00

Table A.6: Summary of combustion tube mixtures.

RUN	Sand (g)	Mesh size (#)	Powdered Kaolinite (g)	(Oil) (g)	Water (g)	Σ (g)
1	7708	60	161	482	482	8833
2	7610	60	151	547	547	8855
3	7404	60	148	503	503	8558
4	7354	60	147	500	500	8501
5	7744	16	155	527	528	8954
6	7870	16	-	535	535	8940
7	7299	60	146	496	496	8437

Table A.7: Cumulative production data for RUN 1.

Time (h) into experiment	Type of liquid	Cumulative amount (g)	Δ (g)
2.63	Water	80.01	80.01
2.98	Water	102.35	22.34
3.13	Water	120.01	17.66

Continued on next page

Table A.7 – continued from previous page

Time (h) experiment	Type liquid	Cum. amount (g) amount (g)	Δ (g)
3.13	Oil	17.17	17.17
3.32	Oil	44.31	27.14
3.58	Oil	77.79	33.48
3.80	Oil	102.73	24.94
4.23	Oil	163.65	60.92
4.95	Oil	231.51	67.86
5.08	Oil	249.51	18.00
∞	Oil	360.40	110.89

Table A.8: Cumulative production data for RUN 2.

Time (h) into experiment	Type of liquid	Cumulative amount (g)	Δ (g)
3.62	Water	20.58	50.58
4.05	Water	91.61	71.03
4.23	Water	114.25	22.64
4.53	Water	144.25	30.00
4.72	Water	177.59	33.34
5.07	Water	229.75	52.16
5.30	Water	265.65	35.90
5.45	Oil	15.99	15.99
5.57	Oil	44.22	24.23
5.68	Oil	83.19	42.97
5.92	Oil	102.73	19.54
5.95	Oil	149.86	47.13

Continued on next page

Table A.8 – continued from previous page

Time (h) experiment	Type liquid	Cum. amount (g) amount (g)	Δ (g)
6.22	Oil	164.35	14.49
6.68	Oil	192.27	27.92
6.72	Oil	232.66	40.39
6.85	Oil	241.22	8.56
6.88	Oil	259.48	18.26
7.05	Oil	281.08	21.60
7.07	Oil	301.83	20.75
7.17	Oil	318.64	16.81
∞	Oil	403.84	85.20

Table A.9: Cumulative production data for RUN 3.

Time (h) into experiment	Type of liquid	Cumulative amount (g)	Δ (g)
2.50	Water	133.04	133.04
2.68	Water	161.85	28.81
2.87	Water	183.02	21.17
3.05	Water	209.66	26.64
3.20	Water	233.65	23.99
3.40	Water	266.68	33.03
3.52	Oil	2.13	2.13
3.67	Oil	25.59	23.46
3.72	Oil	43.53	17.94
3.88	Oil	81.41	37.88
4.05	Oil	129.11	47.70

Continued on next page

Table A.9 – continued from previous page

Time (h) experiment	Type liquid	Cum. amount (g) amount (g)	Δ (g)
4.23	Oil	166.16	37.05
4.37	Oil	192.51	26.35
4.55	Oil	235.24	42.73
4.80	Oil	279.94	44.70
5.00	Oil	313.88	33.94
5.12	Oil	356.88	43.00
5.28	Oil	374.15	17.27
5.55	Oil	455.05	80.90
∞	Oil	457.92	2.87
∞	Condensates	10.44	10.44

Table A.10: Total production data for RUN 5.

Type	Amount (g)
Water	401
Oil	432
Condensate	33.37

Table A.11: Cumulative production data for RUN 6.

Time (h) into experiment	Type of liquid	Cumulative amount (g)	Δ (g)
After Packing	Water	157.77	157.77
During N_2 Injection	Water	219.40	61.63

Continued on next page

Table A.11 – continued from previous page

Time (h) experiment	Type liquid	Cum. amount (g) amount (g)	Δ (g)
1.73	Water	314.94	95.54
2.28	Water	331.55	16.61
4.48	Oil	50.84	50.84
4.66	Oil	76.44	25.60
4.74	Oil	92.87	16.43
4.98	Oil	99.36	6.49
5.34	Oil	114.52	15.16
5.74	Oil	172.93	58.41
∞	Oil	272.79	99.86
∞	Condensates	4.5	4.5

Table A.12: Total production for RUN 7.

Type	Amount (g)
Water	401
Oil	229
Condensate	1

Table A.13: Summary of total production data, RUN 6 failed.

Property	RUN 1	RUN 2	RUN 3	RUN 4	RUN 5	RUN 6	RUN 7
Water (g)	120	266	267	290	401	332	401
Oil (g)	360	404	458	445	432	273	229
Condensates (g)	-	-	10	10	34	5	1

Table A.14: Summary of stoichiometry for HTO reaction, see Eqn. 3.1.

RUN	H/C	O_2	N_2	CO_2	CO	O_2	H_2O	N_2
1	1.25	1.48	5.67	0.75	0.25	0.29	0.63	5.67
2	1.26	1.41	5.41	0.74	0.26	0.23	0.63	5.41
3	1.86	2.65	5.97	0.75	0.25	0.25	0.93	5.97
4	1.37	1.41	5.42	0.74	0.26	0.20	0.69	5.42
5	1.42	1.38	5.28	0.71	0.29	0.17	0.71	5.28
6	2.18	18.26	69.97	0.68	0.32	16.88	1.09	69.97
7	1.45	1.26	4.84	0.75	0.25	0.02	0.72	4.84

Table A.15: Summary of operational data, RUN 6 failed.

Property	RUN 1	RUN 2	RUN 3	RUN 4	RUN 5	RUN 6	RUN 7
Oil Recovery (%)	87	92	93	90	98	82	54
Fuel consumed (g)	58	68	63	65	76	16	59
Overall H/C ratio	1.38	1.38	1.45	1.47	1.54	2.78	1.50
Fuel requirements (kg/m^3)	18.8	23.2	19.6	19.8	27.2	7.8	21.1
Fuel requirements ($kg\ fuel/100\ kg\ sand$)	0.76	0.89	0.85	0.88	0.99	0.2	0.81
Air requirements ($m^3(ST)/m^3$)	248	291	250	244	337	406	236

Table A.16: Summary of gas phase parameters, RUN 6 failed.

Property	RUN 1	RUN 2	RUN 3	RUN 4	RUN 5	RUN 6	RUN 7
H/C ratio	1.25	1.26	1.86	1.37	1.42	2.18	1.45
OFR ($m^3(ST)/m^3$)	2.64	2.51	2.65	2.50	2.43	30.38	2.22
AFR ($m^3(ST)/m^3$)	12.74	12.14	12.82	12.06	11.72	146.78	10.71
f_{O_2R}	0.74	0.73	0.65	0.72	0.71	0.61	0.71
Excess O_2	0.2	0.16	0.14	0.14	0.12	0.92	0.02
Excess air	0.25	0.19	0.16	0.17	0.14	-	0.02
m	3.03	2.87	3.02	2.85	2.41	2.12	3.07

Table A.17: Summary of post mortem analysis.

RUN	Pyrolysis Coke (g)	Burned Zone 1 (g)	Burned Zone 2 (g)	Coke (g)	Transition Zone (g)	Unburned Zone(g)	Total (g)
1	66.16	1529.80	3417.31	85.38	340.54	2332.24	7771.43
2	110.59	350.38	3022.12	30.52	1122.06	1209.79	7620.21
3	80.24	3881.49	1254.06	14.84	1111.85	1223.62	7566.14
4	117.69	2950.07	1951.65	18.78	1046.04	1387.06	7471.29
5	258	3903	1065	92	1121	1545	7984
6	45	1447	410	121	1121	4645	7783
7	54	438	4278	33	1806	998	7607

Appendix B

Additional Figures

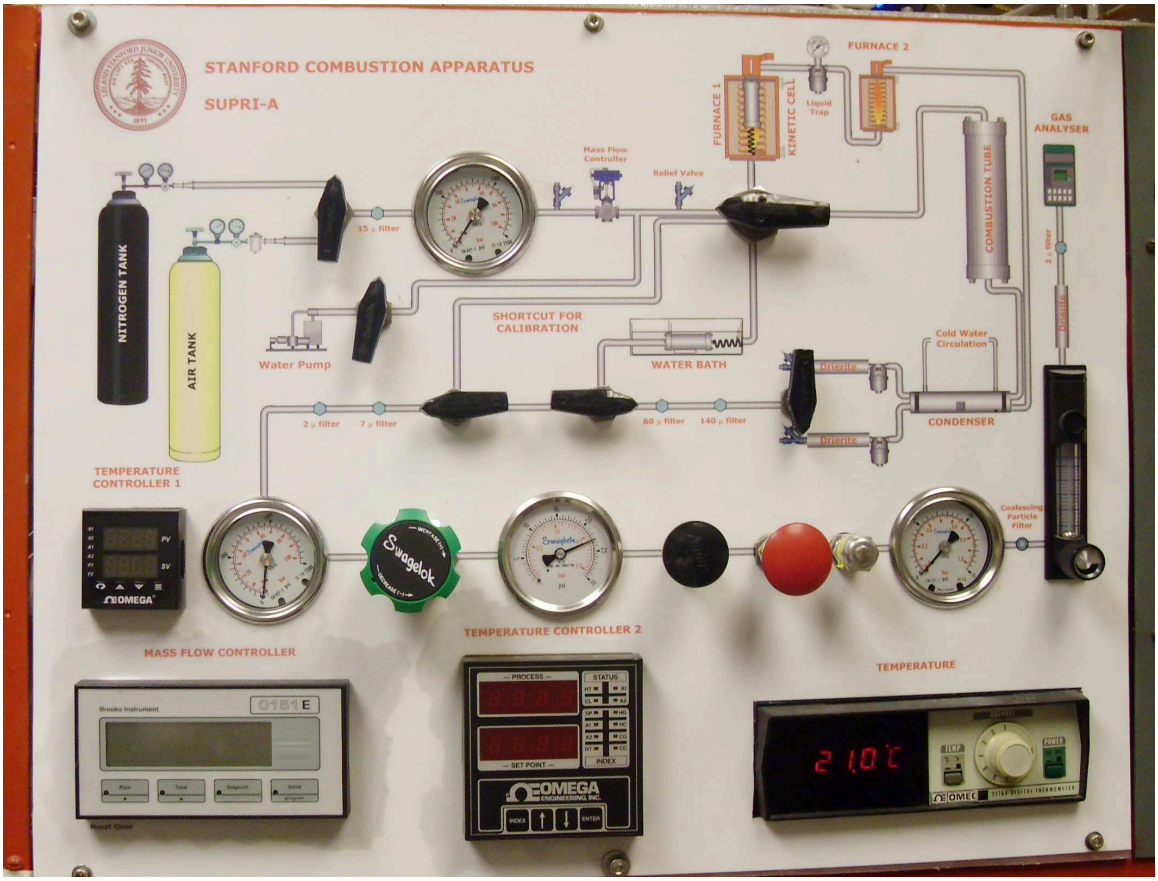

Figure B.1: Experimental apparatus layout.

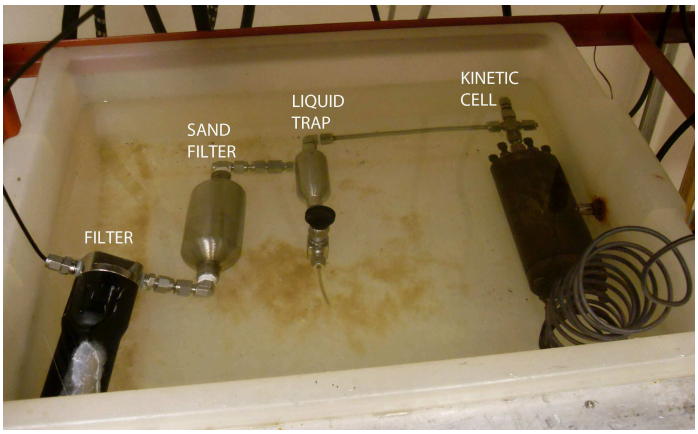

Figure B.2: Leak test of kinetic cell assembly.

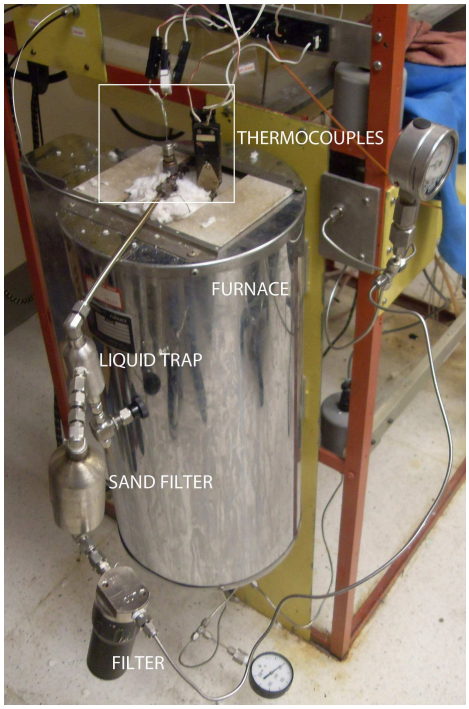

Figure B.3: Furnace with kinetic cell and thermocouples in place.

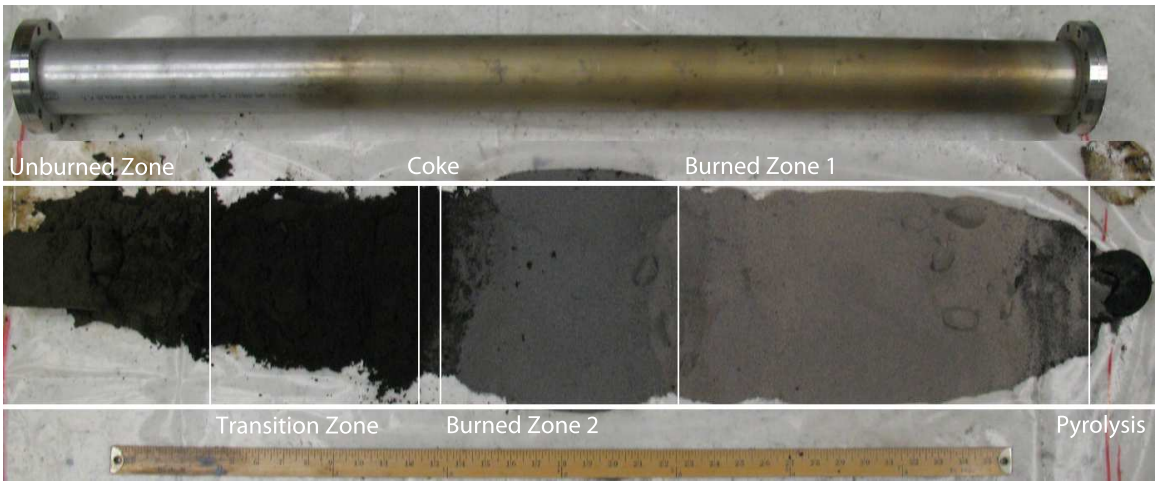

Figure B.4: Post mortem for RUN 2 (mixture given in Table A.6).

Figure B.5: Coke for RUN 2, thickness ≈ 0.5 inch.

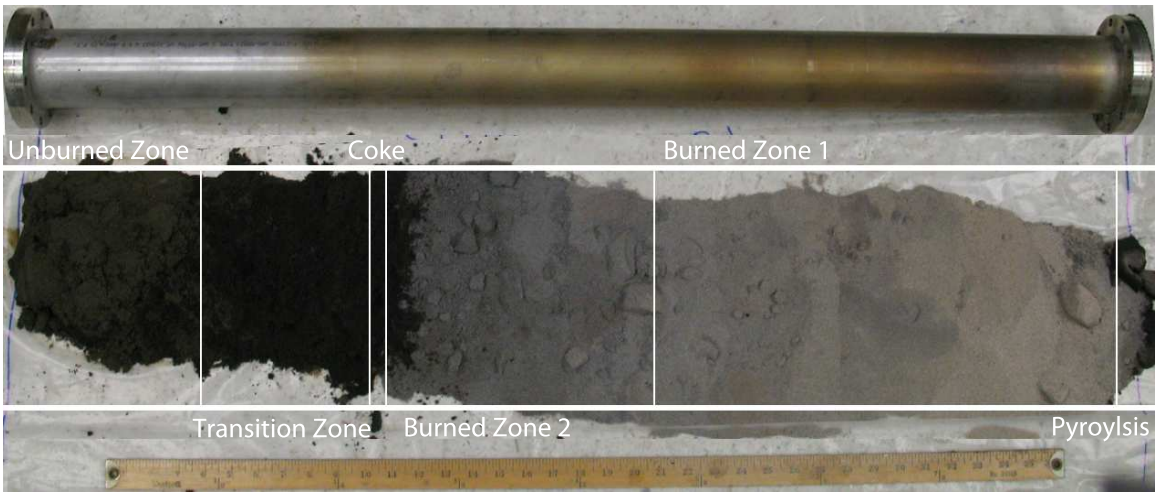

Figure B.6: Post mortem for RUN 3 (mixture given in Table A.6).

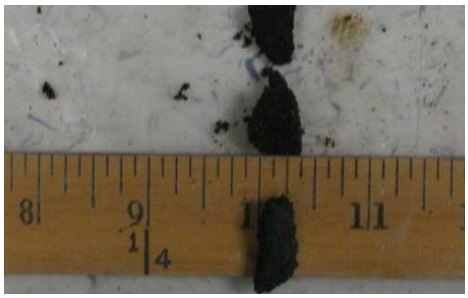

Figure B.7: Coke for RUN 3, thickness ≈ 0.25 inch.

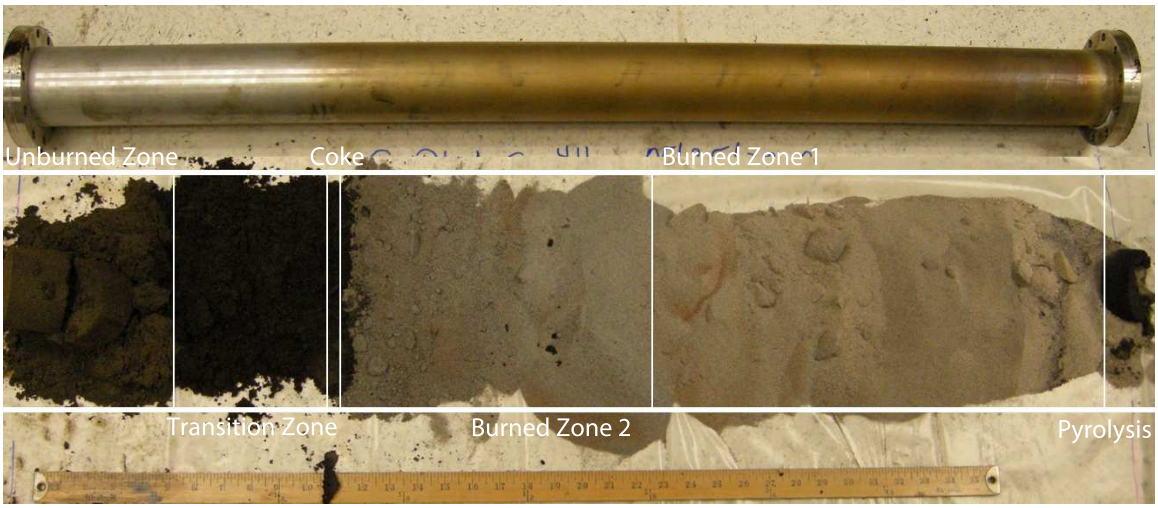

Figure B.8: Post mortem for RUN 4 (mixture given in Table A.6).

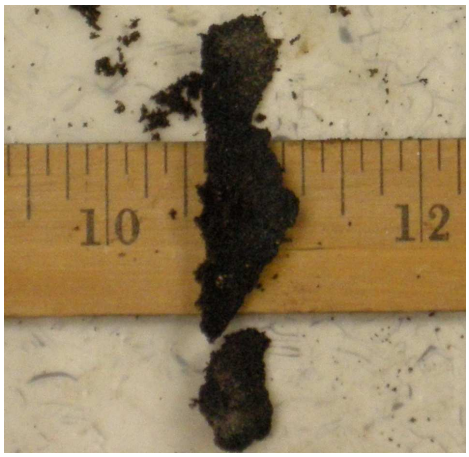

Figure B.9: Coke for RUN 4, thickness ≈ 0.5 inch.

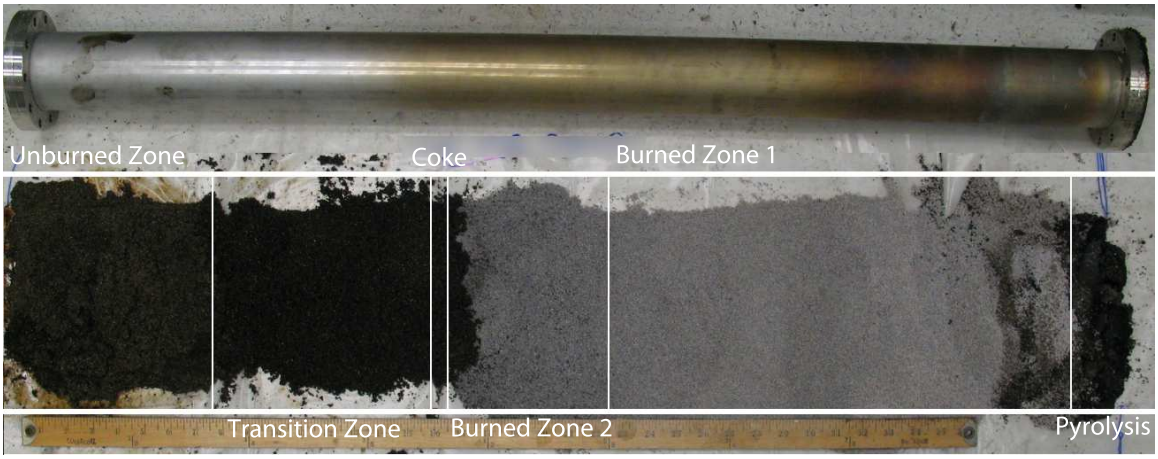

Figure B.10: Post mortem for RUN 5 (mixture given in Table A.6).

Figure B.11: Coke for RUN 5, thickness ≈ 1 inch.

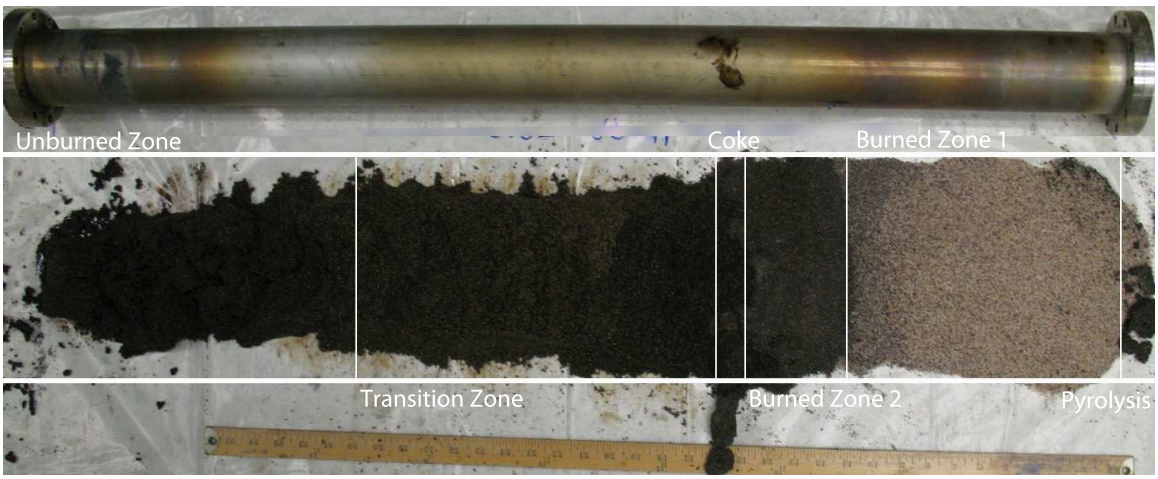

Figure B.12: Post mortem for RUN 6 (mixture given in Table A.6).

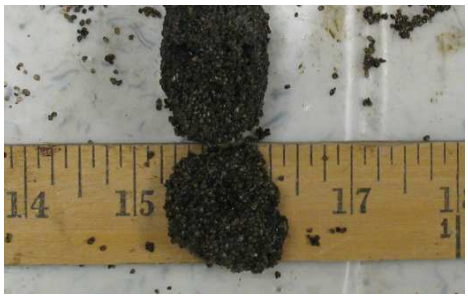

Figure B.13: Coke for RUN 6, thickness $\approx$ 1 inch.

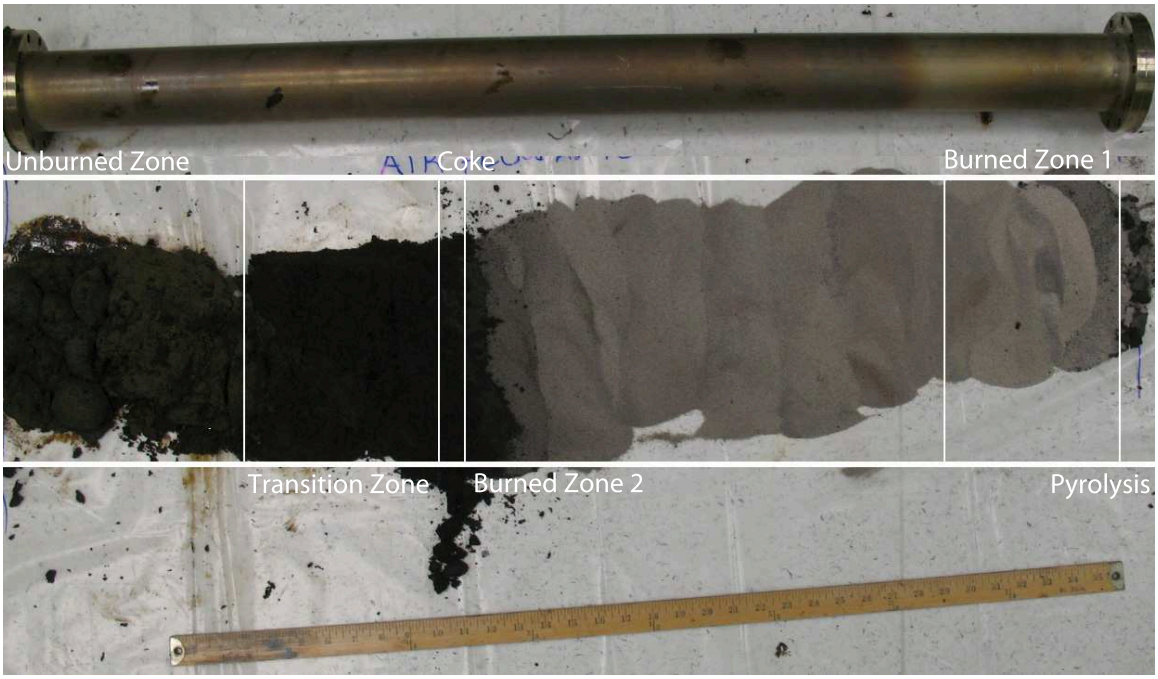

Figure B.14: Post mortem for RUN 7 (mixture given in Table A.6).

Figure B.15: Coke for RUN 7, thickness ≈ 0.5 inch.

Nomenclature

Acronyms

AFR	Air-Fuel Ratio
BOC	Bottom of Cell
COC	Center of Cell
E_a	Apparent/Effective Activation Energy
EOR	Enhanced Oil Recovery
f_{O_2R}	Fraction of the consumed oxygen
H/C	Hydrogen-Carbon Ratio
HTO	High Temperature Oxidation
LTO	Low Temperature Oxidation
m	Molar ratio of CO over CO_2
n	Equivalent atomic H/C ratio of the fuel burned
OFR	Oxygen-Fuel Ratio
R	Ratio of mole fraction of nitrogen to oxygen in feed gas
TOC	Top of Cell

Bibliography

[1] Al-Saffar, H., Price, D., Soufi, A., Hughes, R., *Distinguishing between overlapping low temperature and high temperature oxidation data obtained from a pressurised flow reactor system using consolidated core material.* Fuel, Volume 79, Issue 7, May 2000, Pages 723-732, ISSN 0016-2361, DOI: 10.1016/S0016-2361(99)00210-0.

[2] Ambalea, A. M., Freitag, N. *Thermogravimetric studies on pyrolysis and combustion behaviour of a heavy oil and its asphaltenes.* Energy Fuels 2006, 20, 560565.

[3] Bazargan M., Chen B., Cinar M., Glatz G., Lapene A., Zhu Z., Castanier L., Gerritsen M., and Kovscek A. 2011. A Combined Experimental and Simulation Workflow to Improve Predictability of In Situ Combustion. SPE 144599 presented at the SPE Western Regional Meeting, Society of Petroleum Engineers.

[4] Benham, A. L., Poettman, F. H. *The Thermal Recovery Process - An Analysis of Laboratory Combustion Data.* Journal of Petroleum Technology, Volume 10, Number 9, 1958, 83-85.

[5] Bousaid, I. S., Ramey, H. J., Jr. *Oxidation of crude oil in porous media.* Soc. Pet. Eng. J. 1968, 137148.

[6] Burger, J.G., *Chemical Aspects of In-Situ Combustion - Heat of Combustion and Kinetics.* Institut Francais Du Petrole, SPE Journal, Volume 12, Number 5, October 1972, pp. 410-422.

[7] Burger, J., Sourrieau P., and Combarnous M., *Thermal Recovery Methods.* Editions TECHNIP, Paris France, 1984.

[8] Butler, R.M., *Thermal Recovery of Oil and Bitumen*. Prentice Hall, Englewood Cliffs, New Jersey, 1991.

[9] Burnham, A. K., Dinh, L. N., *A comparison of isoconversional and model-fitting approaches to kinetic parameter estimation and application predictions*. J. Therm. Anal. Calorim. 2007, 89, pp. 479490.

[10] Carcoana, A. *Results and Difficulties of the World's Largest In-Situ Combustion Process: Suplacu de Barcau Field, Romania*. SPE/DOE Enhanced Oil Recovery Symposium, Tulsa, Oklahoma, April 1990.

[11] Carberry, J. J. Chemical and Catalytic Reaction Engineering, McGraw-Hill Book Company, New York, 1976.

[12] M. Cinar, L.M. Castanier, and A.R. Kovscek, 2009. *Isoconversional Kinetic Analysis of the Combustion of Heavy Hydrocarbons*. SPE Western Regional Meeting, 24-26 March 2009, San Jose, California.

[13] Cinar, M., Castanier, L. M., Kovscek, A. R., *Improved analysis of the kinetics of crude-oil in-situ combustion*. In SPE Western Regional Meeting 2008, Bakersfield, CA, March 31-April 2, 2008; SPE Paper 113948.

[14] Cinar, M., Castanier, L.M., and Kovscek, A.R., 2011. *Predictability of Crude Oil In-Situ Combustion by the Isoconversional Kinetic Approach*. To be published in SPE Journal, 2011.

[15] Cinar, M., Castanier, L.M., and Kovscek, A.R., 2011. *Combustion Kinetics of Heavy Oils in Porous Media*. Energy and Fuels, submitted May 2011.

[16] Coats, K. H., *In-situ combustion model*, Soc. Pet. Eng. J., Dec. 1980, 533554.

[17] Coats K.H. 1983. Some Observations on Field-Scale Simulation of the In-Situ Combustion Process. SPE12247 presented at the SPE Reservoir Simulation Symposium, Society of Petroleum Engineers.

[18] Dechelette B., Heugas O., Quenault G., Bothua J., and Christensen J. 2006. Air Injection-Improved Determination of the Reaction Scheme with Ramped Temperature Experiment and Numerical Simulation. Journal of Canadian Petroleum Technology 45(1).

[19] Ewing R. Richard, The Mathematics of Reservoir Simulation, Society for Industrial Mathematics (January 1, 1987).

[20] Farouq Ali, S.M., *A Current Appraisal of In-Situ Combustion Field Tests*. Journal of Petroleum Technology, Volume 24, Number 4, 1972, pp. 477-486.

[21] Fassihi, M.R., W.E. Brigham, and H.J. Ramsey Jr. 1984. *Reaction Kinetics of In Situ Combustion: Part 1 Observation, Part 2 Modelling*. Sot. of Pet. Eng. J. Vol. 24, No. 4, pp. 399416.

[22] Fassihi, M. R. *Analysis of fuel oxidation in in-situ combustion oil recovery*. Ph.D. dissertation, Stanford University, Stanford, CA, April 1981.

[23] Friedman, H. L. *Kinetics of thermal degradation*. J. Polym. Sci., Part C: Polym. Lett. 1964, 6, 183195.

[24] Galwey, A.K., *What is meant by the term 'variable activation energy' when applied in the kinetic analyses of solid state decompositions (crystolysis reactions)?*. Thermochimica Acta, Volume 397, Issues 1-2, 21 February 2003, Pages 249-268, ISSN 0040-6031, DOI: 10.1016/S0040-6031(02)00271-X.

[25] Gates C.F. and Ramey H.J. 1980. A Method for Engineering In-Situ Combustion Oil Recovery Projects. Journal of Petroleum Technology 32(2): 285-294.

[26] Christensen J., Darche G., Dechelette B., Ma H., and Sammon P. 2004. Applications of Dynamic Gridding To Thermal Simulations. SPE 86969 presented at SPE International Thermal Operations and Heavy Oil Symposium and Western Regional Meeting, Society of Petroleum Engineers.

[27] Glatz G., Stanford University, Hasçakir B., Stanford University, Castanier L.M., Stanford University, Clemens T., OMV, Kovscek A.R., Stanford University. Kinetic Cell and Combustion Tube Results for a Central European Crude. SPE 146089-MS, SPE Annual Technical Conference and Exhibition, 30 October-2 November 2011, Denver, Colorado, USA.

[28] Gutierrez D., Skoreyko F., Moore R.G., Mehta S.A., and Ursenbach M.G. 2009. The Challenge of Predicting Field Performance of Air Injection Projects Based on Laboratory and Numerical Modelling. Journal of Canadian Petroleum Technology 48(4): 23-33.

[29] Genrich, J.F., Sohio Petroleum Co.; Pope, G.A., U. of Texas, *A Simplified Performance-Predictive Model for In-Situ Combustion Processes*. SPE Reservoir Engineering, Volume 3, Number 2, 1988, pp. 410-418.

[30] Hasçakir, B., Glatz, G., Castanier, L.M., and Kovscek, A.R., 2011. *In-Situ Combustion Dynamics Visualized With X-Ray Computed Tomography*. SPE J. SPE-135186-PA.

[31] Hundsdorfer W., Jan G. Verwer, Numerical Solutions of Time-Dependent Advection-Diffusion-Reaction Equations, Springer 2007.

[32] *International Energy Outlook*, Report: DOE/EIA-0484(2010), `http://www.eia.doe.gov/oiaf/ieo/`, 2010.

[33] Kristensen M.R. 2008. Development of Models and Algorithms for the Study of Reactive Porous Media Processes. Ph.D. thesis, Technical University of Denmark.

[34] Mamora, D.D., 1993. *Kinetics of in-situ combustion*. Ph.D. Thesis, Stanford, CA: Stanford University.

[35] Mamora, D.D., *New Findings in Low-Temperature Oxidation of Crude Oil*. SPE 293-24, March, 1995.

[36] Marjerrison D. and Fassihi M. 1992. A Procedure for Scaling Heavy-Oil Combustion Tube Results to a Field Model. SPE 24175 presented at the SPE/DOE Enhanced Oil Recovery Symposium, Society of Petroleum Engineers.

[37] Moore, R.G., *New Strategies for In-Situ Combustion*. J. Can. Pet. Tech., Vol.32, No. 10, December, pp. 11-13.

[38] Moore, R.G., Ursenbach, M.G., Laureshen, C.J., and Mehta, S.A., 1997. *Observation and Design Considerations for In-Situ Combustion*. SPE, 97-100.

[39] Moore, R.G., Laureshen, C.J., Ursenbach, M.G., Mehta,, S.A., Belgrave, J.D.M., U. of Calgary, *Combustion/Oxidation Behavior of Athabasca Oil Sands Bitumen*. SPE Reservoir Evaluation & Engineering, Volume 2, Number 6, December 1999, pp. 565-571.

[40] Morten, R. K., *Development of Models and Algorithms for the Study of Reactive Porous Media Processes*, Technical University of Denmark, Department of Chemical and Biochemical Engineering, Frydenberg A/S, Copenhagen, Denmark, 2008.

[41] Oyekonwu, M.O., Pande, K., Ramey, H.J., and Brigham, W. E., 1986. *Experimental and simulation studies of laboratory in-situ combustion recovery*. Paper SPE 15090, SPE 56th California Regional Meeting, Oakland, CA, April 2-4, pp. 483-496.

[42] Paduraru, R., Pantazi, I. IOR/EOR - Over Six Decades of Romanian Experience, Institute for Research and Technology (ICPT), SPE European Petroleum Conference, Paris, France, October 2000.

[43] Prasad, R. S., Slater, J. A. High Pressure Combustion Tube Tests, SPE/DOE 14919, Presented at the 5th SPE/DOE Symposium on Enhanced Oil Recovery. Tulsa, Oklahoma, April 20-23, 1986

[44] Prats, M., Thermal recovery, Henry L. Doherty Series, monograph vol. 7, SPE, 1986.

[45] Petit, H.J-M., Le Thiez, P., Lemonnier, P., *History Matching of a Heavy-Oil Combustion Pilot in Romania*. SPE/DOE Enhanced Oil Recovery Symposium, Tulsa, Oklahoma, April 1990.

[46] Ren, S. R., Greaves, M., Rathbone, R. R., *An IOR Technique for Light-Oil Reservoirs*, SPE Journal, Volume 7, Number 1, pp. 90-99, March 2002.

[47] Rubin, Barry, Buchanan, W. Lloyd, Computer Modelling Group, 1985.*A General Purpose Thermal Model*. SPE Journal, Volume 25, Number 2, 202-214.

[48] Sarathi, P. *In-Situ Combustion Handbook Principles and Practices*; National Petroleum Technology Office: Tulsa, OK, 1999; Report DOE/PC/91008-0374, OSTI_ID 3174.

[49] Savitzky, A., Golay, M. J. E., *Smoothing and Differentiation of Data by Simplified Least Squares Procedures*. Analytical Chemistry, Volume 36, Number 8, 1627-1639, 1964.

[50] Eclipse[1] software version 2009 Software Manual. Schlumberger Ltd.

[51] Semenov, N. *Chemical Kinetics and Chain Reactions*. Oxford University Press: London, U.K., 1935.

[52] Shirley, D.A., Phys. Rev. B 5, 4709-4714, 1972.

[53] Smith, J. M. Chemical Engineering Kinetics, McGraw-Hill Book Company, New York, 1970.

[54] Vyazovkin, S., *Reply to "What is meant by the term 'variable activation energy' when applied in the kinetics analyses of solid state decompositions (crystolysis reactions)?"*. Thermochimica Acta, Volume 397, Number 1, 21 February 2003 , pp. 269-271(3).

[55] Wefer G., David Billet, Dierk Hebbeln, Bo B. Jorgensen, Michael Schlter, Tjeerd C.E. Van Weering. Ocean Margin Systems, Springer; 1 edition (November 4, 2002).

[1]Mark of Schlumberger

[56] Vyazovkin, S. Isoconversional kinetics in: The handbook of thermal analysis & calorimetry, Vol.5 Eds. M. E. Brown, P. K. Gallagher, Elsevier, Amsterdam, 2008, pp. 503-538.

[57] Z. Zhu, M. Bazargan, A. Lapene, M. Gerritsen, L. Castanier, and A. Kovscek, SPE, Stanford University, Upscaling for Field-scale In-situ Combustion Simulation, SPE Western North American Region Meeting, 7-11 May 2011, Anchorage, Alaska, USA.